

UNIVERSITY OF CALIFORNIA

Radiation Laboratory
Berkeley, California

Contract No. W-7405-eng-48

THE ANTIPROTON-NUCLEON ANNIHILATION PROCESS
(ANTIPROTON COLLABORATION EXPERIMENT)

W. H. Barkas, R. W. Birge, W. W. Chupp, A. G. Ekspong, G. Goldhaber,
S. Goldhaber, H. H. Heckman, D. H. Perkins, J. Sandweiss, E. Segrè,
F. M. Smith, D. H. Stork, and L. Van Rossum

Radiation Laboratory and Department of Physics
University of California, Berkeley, California

and

E. Amaldi, G. Baroni, C. Castagnoli, C. Franzinetti, and A. Manfredini

Istituto di Fisica della Universita, Roma
Istituto Nazionale di Fisica Nucleare,
Sezione di Roma, Italy

September 10, 1956

THE HISTORY OF THE

REPUBLIC OF THE UNITED STATES

OF AMERICA

FROM THE FIRST SETTLEMENTS TO THE PRESENT TIME

BY

WILLIAM STUBBS

AND

WALTER DE RUIJTER

LONDON

ANTIPROTON-NUCLEON ANNIHILATION EXPERIMENT

Contents

Abstract	4
I. Introduction	6
II. Experimental Procedure	
A. The Exposure at the Bevatron	8
B. Scanning Procedure.	8
III. Measurements on the Primary P ⁻ Tracks	
A. Antiproton Mass Estimates	11
1. Range vs Momentum.	11
2. Track Opacity vs Residual Range	12
3. Grain Density vs Multiple Scattering	14
B. The Antiproton Interaction Cross Section	
1. The Cross-Section Determination	14
2. Elastic Scattering	18
3. The Antiproton Cross Section at Low Velocities	20
a. Determination of the residual range	20
b. Variation of cross section with velocity	21
IV. The Antiproton Annihilation Process	
A. The Visible Energy Release in the Annihilation Stars	23
B. The Pion Spectrum	23
C. The Nuclear Excitation	
1. The Energy Given to Nucleons	27
2. Correlation of Charged Pion Multiplicity and Energy Transfer to Nucleons	31
3. Pion Interactions.	31
D. K-Meson Production in Annihilation Stars	34
E. Angular Distribution of Pions	35
F. Properties of Annihilation Stars.	35
1. The Energy Balance.	38
2. The Average Pion Multiplicity	39
G. Comparison with Statistical Theories	41
1. The Fermi Statistical Model	42
2. The Pion Energy Distribution	42
3. The Lepore-Neuman Statistical Model.	44
4. Consequences of I-Spin Conservation	46

H. Discussion on the Annihilation Radius.	49
Acknowledgments.	50
Appendices	
I. Examples of Antiproton Annihilation Stars	51
Event 3-13: 5 charged pions	
Event 4-8: 4 charged pions	
Event 1-2: 3 charged pions	
Event 3-2: 2 charged pions, inelastic scattering of p^-	
Event 1-1: 2 charged pions	
Event 4-10: 1 charged pion	
Event 4-3: no charged pions	
Event 5-1: no charged pions, possible charge exchange	
II. Evidence for K-Meson Production. (By A. Gösta Eksping and Gerson Goldhaber).	68
1. Event 3-3: Evidence for the production of a $K\bar{K}$ meson pair in the annihilation process	
2. Event 3-7: Evidence for the emission of one charged K meson from an annihilation star	
III. Annihilation Accompanied by K-Particle Production and with Accountable Energy and Momentum. (By Harry H. Heckman).	78
Event 2-3	
IV. Measurements of Multiple Scattering on Steep Tracks	
A. The Grid-Coordinate Method.	84
B. The Surface-Angle Method	85
V. The Lepore-Neuman Statistical Model	87
Figure Captions	89

THE ANTIPROTON-NUCLEON ANNIHILATION PROCESS
(ANTIPROTON COLLABORATION EXPERIMENT)

W. H. Barkas, R. W. Birge, W. W. Chupp, A. G. Ekspong, G. Goldhaber,
S. Goldhaber, H. H. Heckman, D. H. Perkins, J. Sandweiss, E. Segrè,
F. M. Smith, D. H. Stork, and L. Van Rossum

Radiation Laboratory and Department of Physics
University of California, Berkeley, California

and

E. Amaldi, G. Baroni, C. Castagnoli, C. Franzinetti, and A. Manfredini

Istituto di Fisica della Universita, Roma
Istituto Nazionale di Fisica Nucleare,
Sezione di Roma, Italy

September 10, 1956

ABSTRACT

In the exposure to a 700-Mev/c negative particle beam, 35 antiproton stars have been found. Of these antiprotons, 21 annihilate in flight and three give large-angle scatters ($\theta > 15^\circ$, $T_{p^-} > 50$ Mev), while 14 annihilate at rest. From the interactions in flight we obtain the total cross section for antiproton interaction

$$\sigma_{p^-}/\sigma_0 = 2.9 \pm 0.7,$$

where $\sigma_0 = \pi R_0^2$ and $R_0 = 1.2 \times 10^{-13} A^{1/3}$ cm. This cross section was measured at an average antiproton energy of $\bar{T}_{p^-} = 140$ Mev.

We also find that the antiproton-nucleon annihilation proceeds primarily through pion production with occasional emission of K particles. On the average 5.3 ± 0.4 pions are produced in the primary process; of these 1 pion is absorbed and 0.3 inelastically scattered. From the small fraction of pions absorbed we conclude that the annihilation occurs at the surface of the nucleus at a distance larger than the conventional radius.

A total energy balance of particles emitted in the annihilation gives a ratio of charged to neutral pions consistent with charge independence. Conversely, assuming charge independence, we conclude that the energy going into electromagnetic radiation or neutrinos is small.

Comparisons with the Fermi statistical model and the Lepore-Neuman statistical model have been made. Good agreement with the experimental results on the annihilation process can be obtained through appropriate choice of the interaction volume parameters.

THE ANTIPROTON-NUCLEON ANNIHILATION PROCESS*
(ANTIPROTON COLLABORATION EXPERIMENT)

W. H. Barkas, R. W. Birge, W. W. Chupp, A. G. Ekspong, † G. Goldhaber,
S. Goldhaber, H. H. Heckman, D. H. Perkins,⁶ J. Sandweiss, E. Segrè,
F. M. Smith, D. H. Stork, and L. Van Rossum**

Radiation Laboratory and Department of Physics
University of California, Berkeley, California

and

E. Amaldi, G. Baroni, C. Castagnoli, C. Franzinetti, and A. Manfredini
Istituto di Fisica della Universita, Roma
Istituto Nazionale di Fisica Nucleare,
Sezione di Roma, Italy

September 10, 1956

I. INTRODUCTION

A program for the search for and study of antiprotons in emulsions was initiated^{1, 2} concurrently with the counter experiment at the Berkeley Bevatron that demonstrated the existence of antiprotons.³ The first aim of the emulsion program was to provide the proof for the annihilation process. This was recently accomplished⁴ when the first star observed in the exposure discussed here gave a visible energy release greater than $M_p c^2$. Once the proof

* This work was done under the auspices of the U. S. Atomic Energy Commission.

† Now at the University of Uppsala, Uppsala, Sweden.

⁶ Now at the University of Bristol, Bristol, England.

** Supported in part by a grant from the National Academy of Sciences.

¹ Chamberlain, Chupp, Goldhaber, Segrè, Wiegand, Amaldi, Baroni, Castagnoli, Franzinetti, and Manfredini, Phys. Rev. 101, 909 (1956), and Nuovo Cimento 3, 447 (1956).

² Stork, Birge, Haddock, Kerth, Peterson, Sandweiss, and Whitehead, unpublished. This exposure employed a separated beam using a beryllium absorber. Star 4-8 in our compilation came from this exposure.

³ Chamberlain, Segrè, Wiegand, and Ypsilantis, Phys. Rev. 100, 947 (1955).

⁴ Chamberlain, Chupp, Ekspong, Goldhaber, Goldhaber, Lofgren, Segrè, Wiegand, Amaldi, Baroni, Castagnoli, Franzinetti, and Manfredini, Phys. Rev. 102, 921 (1956).

was provided, the emphasis in this work was shifted to a study of the annihilation process and the antiproton interactions in nuclear emulsion.

In the exposure to the 700-Mev/c negative-particle beam that is now being studied, 35 antiproton stars have been found. The statistical analysis of these stars is discussed in this paper.

We will show that the antiproton-nucleon annihilation proceeds primarily through pion production, with occasional emission of K particles; on the average, 5.3 ± 0.4 pions are produced. Energy is then transferred to the nucleus as a secondary reaction involving the absorption of one pion and the inelastic scattering of 0.3 pion, on the average. The small fraction of absorbed pions leads us to believe that the annihilation is predominantly a surface phenomenon. Indeed, annihilation frequently occurs at a distance from the center of the nucleus that is greater than the conventional nuclear radius. This annihilation, occurring in the region of reduced nuclear density,⁵ is undoubtedly directly related to the large annihilation cross section observed for antiprotons.⁶ This large cross section is confirmed by the results of our experiment.

We have also evaluated the fraction of energy going into nucleons, charged pions, and K mesons. When the remaining energy is assumed to go into neutral pions, the ratio of $\pi^\pm : \pi^0$ is consistent with charge independence. Conversely, if charge independence holds in the antiproton-nucleon annihilation, we can conclude that the energy going into electromagnetic radiation or neutrinos must be small.

A careful examination of the elastic scattering of the antiprotons suggests a possible destructive interference between nuclear and Coulomb scattering.

Finally, theoretical calculations based on the Fermi Statistical Model have been made. For the Fermi theory we have computed the energy spectrum and, more significant, the expected multiplicities of pions and K mesons for different choices of the only available parameter; the interaction volume Ω . We find that the experimental data fit the calculation for $\Omega = 12 \left[\frac{4}{3} \pi \left(\frac{\hbar}{m_\pi c} \right)^3 \right]$ corresponding to an interaction radius of about $2.3 \frac{\hbar}{m_\pi c}$. Calculations have also been performed using the Lepore-Neuman model with similar results.

⁵Hahn, Ravenhall, and Hofstadter, Phys. Rev. 101, 1131 (1956). M. A. Melkanoff, S. A. Moszkowski, J. Nodvik, and D. S. Saxon, Phys. Rev. 101, 507 (1956).

⁶Chamberlain, Keller, Segrè, Steiner, Wiegand, and Ypsilantis, Phys. Rev. 102, 1637 (1956).

II. EXPERIMENTAL PROCEDURE

A. The Exposure at the Bevatron

Three stacks of nuclear emulsions were exposed in the 700-Mev/c negative-particle beam at the Bevatron (Stacks 67, 68, and B). This momentum was chosen in order to obtain good visual discrimination between antiprotons and pions at the leading edge of our stacks. At this momentum protons are at twice minimum ionization, while pions are essentially at minimum ionization. The stack size (7 in. in beam direction by 4 by 3 in.) was chosen to stop the antiprotons well inside the stack. Further details of the experimental setup are contained in a previous communication.⁴ The exposure was remarkably successful in eliminating confusing background particles (p^+). This was achieved by use of a clearing magnet and by both good collimation and momentum definition. Under these conditions we were able to find 35 antiprotons in these stacks despite a background of negative pions in the ratio of $\pi^-/p^- \approx 5 \times 10^5$.

B. Scanning Procedure

The good collimation and momentum definition permitted us to select antiproton tracks on the basis of grain density and angles of entrance relative to pions, at the leading edge of the stack. In addition to the above criteria, the identification of antiprotons was based on the terminal behavior and the range of the particle (the latter applies only to antiprotons coming to rest).

The emulsions were scanned under 22x to 53x objectives with 10x eyepieces. The method of scanning was to traverse each sheet of emulsion perpendicular to the beam direction at about 4mm from the leading edge. When a track at about twice minimum ionization and satisfying the angular entrance criteria was detected, it was followed until it either interacted in flight or came to the end of the range.

The direction of the antiprotons was well collimated about 0° with a standard deviation of $0.9^\circ \rightarrow 0.2^\circ$. The entrance directions are defined as the projected and dip angles measured relative to the mean pion direction at the point of entrance. The small cone of angular acceptance enhanced the speed of scanning, as very few background tracks satisfied the selection criteria (see Table IV, Section III-B-1).

The plates were scanned in Berkeley and in Rome. Thirty-two stars were found in Berkeley, and three stars in Rome.⁷ The first number of the code identifying each star refers to the workers by whom the star was found and analyzed. The workers are designated thus.

At Berkeley,

1. W. W. Chupp and S. Goldhaber;
2. W. H. Barkas, H. H. Heckman, and F. M. Smith;
3. A. G. Ekspong and G. Goldhaber;
4. R. W. Birge, D. H. Perkins, J. Sandweiss, D. H. Stork, and L. Van Rossum.

At Rome,

5. E. Amaldi, G. Baroni, C. Castanoli, C. Franzinetti, and A. Manfredini.

⁷Three additional stars were found in other exposures. Two of these stars were found at Berkeley (Event 4-8--see Ref. 2; and event 4-10--see Table VIII a). One of these stars was found at Rome (event BR 1--see Ref. 1).

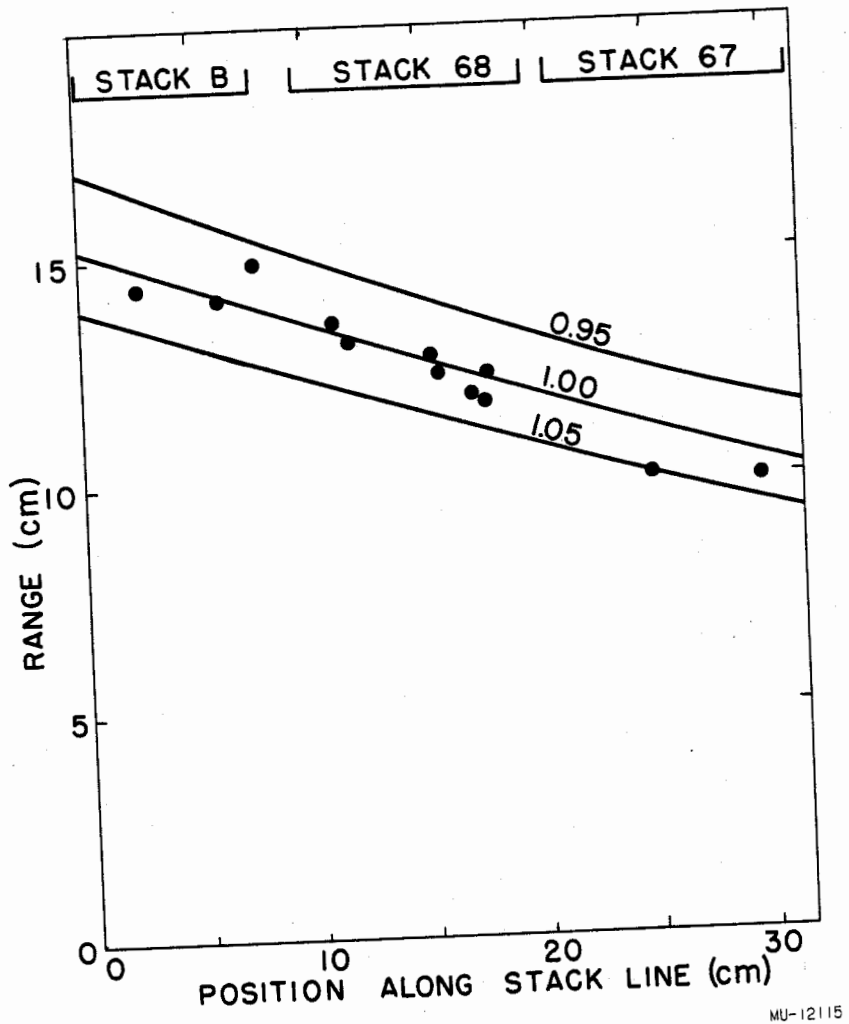


Fig. 1

III. MEASUREMENTS ON THE PRIMARY ANTIPROTON TRACKS

A. Antiproton Mass Estimates

The procedure we have used for finding antiproton tracks in the emulsion stacks constitutes a mass measurement. Because all the particles entering the emulsion stack at the same point have substantially the same momentum, the rate of energy loss—as determined from grain density of track—is a measure of the particle velocity and hence of its mass. Unfortunately, the measurement of grain density is rather subjective, and for a good mass determination it would have been necessary to normalize and stabilize the grain counting by each observer. Since this was not done, the initial grain counts did not provide the best estimates of the antiproton mass.

The methods that were used are summarized in this section, and—as will be seen—the results indicate that the particles being studied form a group whose mass is that of the proton. Some of the methods are applicable only to the particles that come to rest in the emulsion; these are the most reliable.

1. Range vs Momentum

The range of a particle for a given momentum is determined by the particle mass. In this experiment, the antiproton momenta are directly related to the points of entry of the particles into the emulsion stack, and can be determined from the geometry and the strength of the analyzing fields as obtained from wire orbit measurements. Figure 1 shows the observed ranges plotted against the points of entry. The calculated ranges for particles of mass 0.95, 1.00, and 1.05 proton masses are shown as curves on the same plot.

The experimental range straggling of $\pm 4\%$ is too high to arise from Bohr straggling alone. However, the geometry of the exposure is such that a momentum spread of approximately $\pm 1.3\%$ is reasonable. The latter causes most of the observed range straggling. The apparent mass of each antiproton for which the range has been determined is listed in Table I, giving a mean of 1.010 ± 0.006 proton masses; the error quoted is the statistical standard error. A conservative upper limit to the possible systematic error in the momentum determination is 2% resulting in a 3% uncertainty in the mass. Other possible sources of systematic error come from uncertainties in the

emulsion density and in the range-momentum relationship employed.⁸ This type of measurement is the best of those performed up to now to show the uniqueness of the mass of the antiproton.

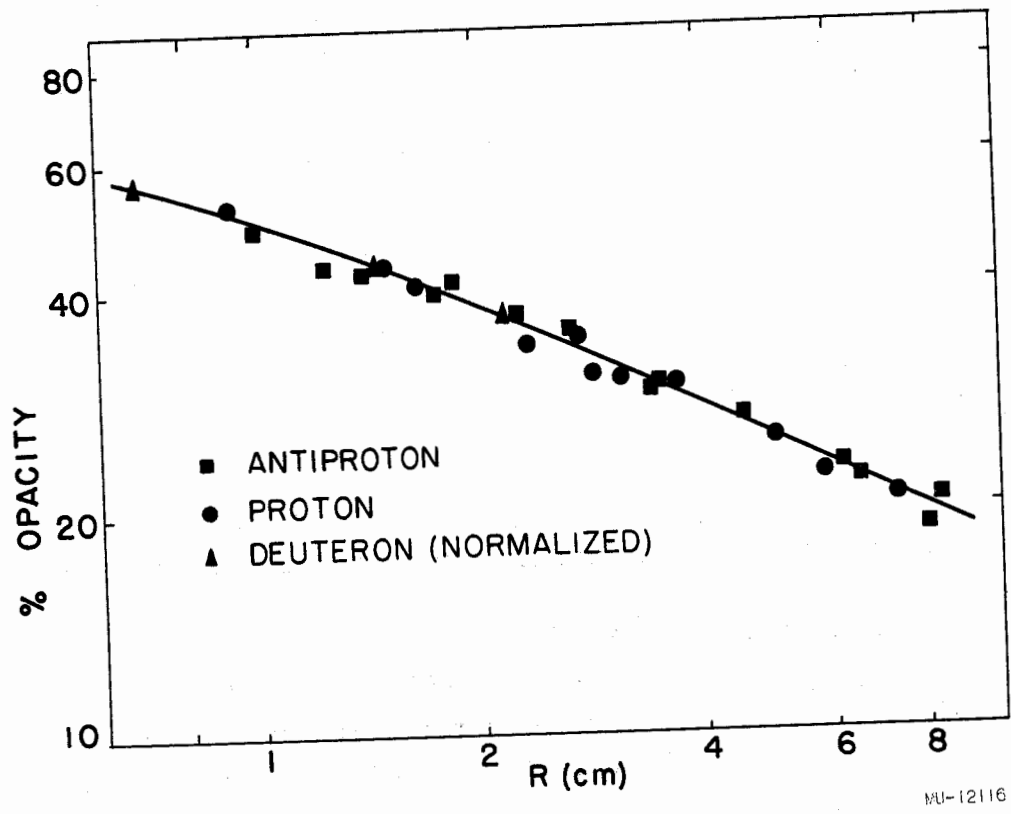
Table I. Antiproton mass measurements by residual range and momentum.

Particle number	Mass (proton masses)
1-2	0.995
1-3	0.998
1-5	1.025
2-1	1.003
2-2	1.017
2-5	0.965
3-1	1.012
3-6	1.023
3-9	1.006
3-13	0.994
4-3	1.023
5-3	1.053

2. Track Opacity vs Residual Range

The mass of a particle can be determined also from its rate of energy loss and residual range. One of the objective measures of the rate of energy loss is the track opacity, or average fraction of the length of a track element occupied by silver grains. Calibration was achieved by making measurements of opacities of proton and deuteron tracks as a function of residual range in the same emulsion as the antiprotons. Because the rate of energy loss is a function of the range divided by the mass, the deuteron ranges have been divided by two and plotted with the protons and antiprotons in Fig. 2. The antiproton masses measured in this way are listed in Table II. Their average is 1.009 ± 0.027 proton masses.

⁸Barkas, Heckman, and Smith, Bull. Amer. Phys. Soc. No. 4, Series II 1 (1956); also Walter H. Barkas, Preliminary Calculations: Range-Energy Curve for Protons in G. 5 Emulsion of Density 3.815 g/cm^2 (High-Velocity Portion), UCRL-3384, April 1956.



MU-12116

Fig. 2

Table II. Antiproton masses
measured by track opacity and residual range

Particle number	2-1	2-4	2-5	3-1	4-3
Mass (proton masses)	0.937 ± 0.055	1.077 ± 0.048	1.021 ± 0.048	0.97 ± 0.10	0.93 ± 0.11

3. Grain Density vs Multiple Scattering

For antiprotons that do not come to rest in the emulsion, the best mass estimate that we could make without invoking the momentum measurements is one derived from the observed grain density and multiple scattering. This method has been applied to a number of antiprotons, most of which annihilate in flight. The results are shown in Table III. The average mass obtained is 0.999 ± 0.043 .

Table III. Masses of antiprotons in units of the proton
determined by grain density and multiple scattering

Particle number	2-3	4-2	4-3	4-4	4-5
Mass (proton masses)	1.04 ± 0.1	1.10 ± 0.14	1.00 ± 0.08	0.95 ± 0.08	0.98 ± 0.11

By combining the results from Sections 2 and 3 above, which do not depend on the particle momentum measurements, we obtain 1.004 ± 0.025 for the antiproton mass in units of the proton. Although we know of no large systematic errors in these measurements, past experience indicates that systematic errors of as much as 3% may be present.

B. The Antiproton Interaction Cross Section

1. The Cross-Section Determination

The method of scanning along the track of antiprotons permitted us to observe antiprotons from the point where they were selected ($T_p \approx 230$ Mev)

up to the point where they interacted. In Stacks 67, 68, and B we have followed 35 p^- tracks. Of these antiprotons, 21 annihilated in flight and three gave large-angle scatters ($\theta > 15^\circ$, $T_{p^-} > 50$ Mev, see Table IV for details), while 14 survived to the ends of their ranges, annihilating at rest. The path length of p^- track followed was 300 ± 30 cm. The uncertainty arises from those tracks that left the stack, some of which might have been positive protons. In addition to the 35 identified antiprotons, two particles satisfying the selection criteria came to rest with no visible stars and were assumed to be positive protons. We have assumed that the same fraction of those particles leaving the stack were also positive protons (see Table V for details). The corresponding mean free paths in emulsions are $\lambda_{\text{annih}} = 14.3 \pm 3.4$ cm and $\lambda_{\text{tot}} = 12.5 \pm 2.8$ cm, where the errors are the statistical standard errors combined with the 10% uncertainty in the path length followed. These values of the mean free path are for the average kinetic energy

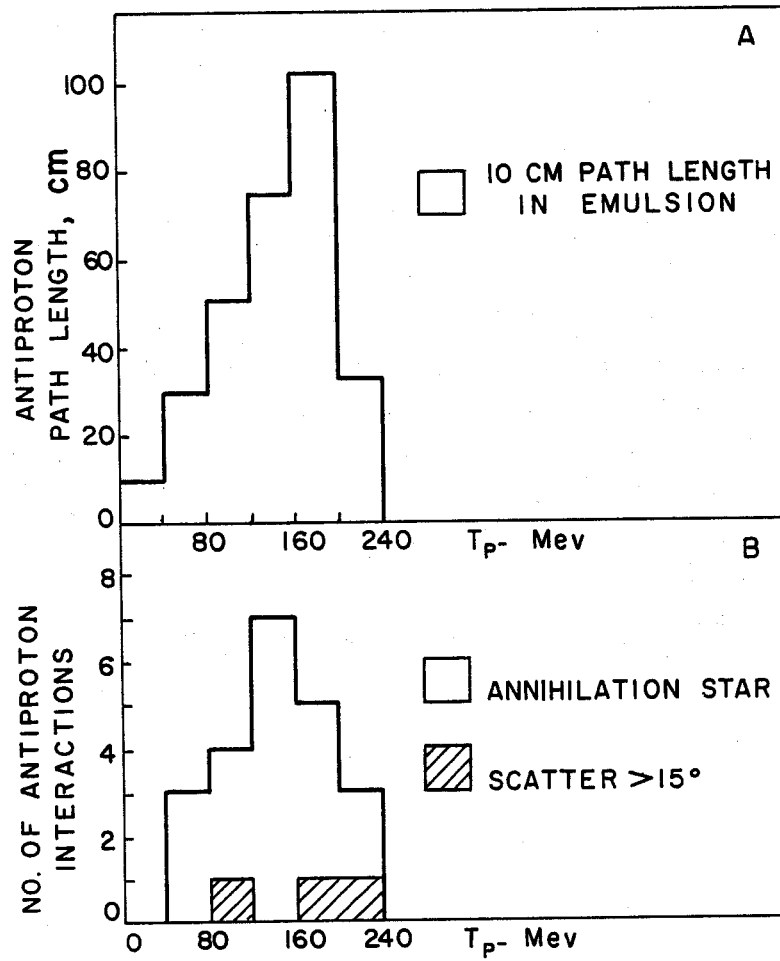
$$\bar{T}_{p^-} = \frac{\int_{20}^{240} T_{p^-} \left(\frac{dT}{dR}\right)^{-1} dT}{\int_{20}^{240} \left(\frac{dT}{dR}\right)^{-1} dT}.$$

This integration was carried out numerically over the observed path-length distribution as shown in Fig. 3A, and gives $\bar{T}_{p^-} = 140$ Mev. Figure 3B gives the distribution of annihilation and scattering events over the same energy interval.

It is interesting to compare the resulting nuclear radius and nuclear cross section for antiproton interactions with the corresponding values obtained in this laboratory for Cu and Be with a counter technique at $T_{p^-} \approx 500$ Mev.⁶ Our present value for the total cross section is $\sigma_{p^-}/\sigma_0 \approx 2.9 \pm 0.7$, where $\sigma_0 = \pi R_0^2$ and $R_0 = 1.2 \times 10^{-13} A^{1/3}$ cm, while at the higher energy we have $\sigma_{p^-}/\sigma_0 \approx 2$ (see Table VI for details).

All the interactions observed were either annihilation or scattering events except for one which was an interaction in flight, with an energy release $E_{\text{vis}} < T_{p^-}$ (Event 5-1, given in detail in Appendix I). This event can be interpreted as one of the following:

- (a) a charge-exchange scattering, $p^- + "p" \rightarrow \bar{n} + "n"$;
- (b) an annihilation in flight with no charged pion emission (compare with Event 4-3, Appendix I);
- (c) the interaction of a background positive proton.



MU-12117

Fig. 3

Only one event of this type has been observed out of a total of 24 interactions in flight, hence we conclude that charge-exchange scattering of anti-protons occurs in only a small fraction of the interactions in nuclear emulsion.

Table IV. Observed nuclear scatters of antiprotons

Event No.	T_{p^-} (Mev)	Scattering angle (degrees)	ΔT_{p^-} (Mev)
1-3	82	53	~ 0 (Elastic)
3-2 ^a	163	47	~ 31 (Inelastic)
1-4 ^b	224	16	~ 14 (Inelastic)

^aEvent 3-2 is given in detail in Appendix I.

^bIn Event 1-4 the track leaves the stack before coming to rest; its identity as a p^- scatter is thus not definitely established.

Table V. Details for tracks followed and antiproton interactions in Stacks 67, 68, and B

	No. followed	Path length (cm)	No. annihilated in flight	No. scattered in flight
Identified p^- tracks followed	35	260	21	2
Possible p^- tracks followed (tracks leaving stack)	7	47	-	1
Possible p^- tracks followed (ending as p_ρ particles)	2	23	-	-
Total	44	330	21	3
Estimated p^- path-length		300 ± 30		

Table VI. Comparison of antiproton interaction cross sections and effective radii for $T_{p^-} = 500 \text{ Mev}^a$ and $T_{p^-} = 140 \text{ Mev}$ (our data)

T_{p^-} (Mev)	Elements	Cutoff angle (degrees)	r_{p^+} (10^{-13} cm)	r_{p^-} (10^{-13} cm)	σ_{p^-}/σ_0^b
500 ^a	Be	18	1.14±0.04	1.63±0.14	1.85±0.30
500 ^a	Cu	12.7	1.24±0.06	1.77±0.12	2.18±0.30
140	Emulsion	15	-	2.05±0.23	2.91±0.7
140	Emulsion	annihilation only	-	1.92±0.23	2.56±0.6

^aReference 6.

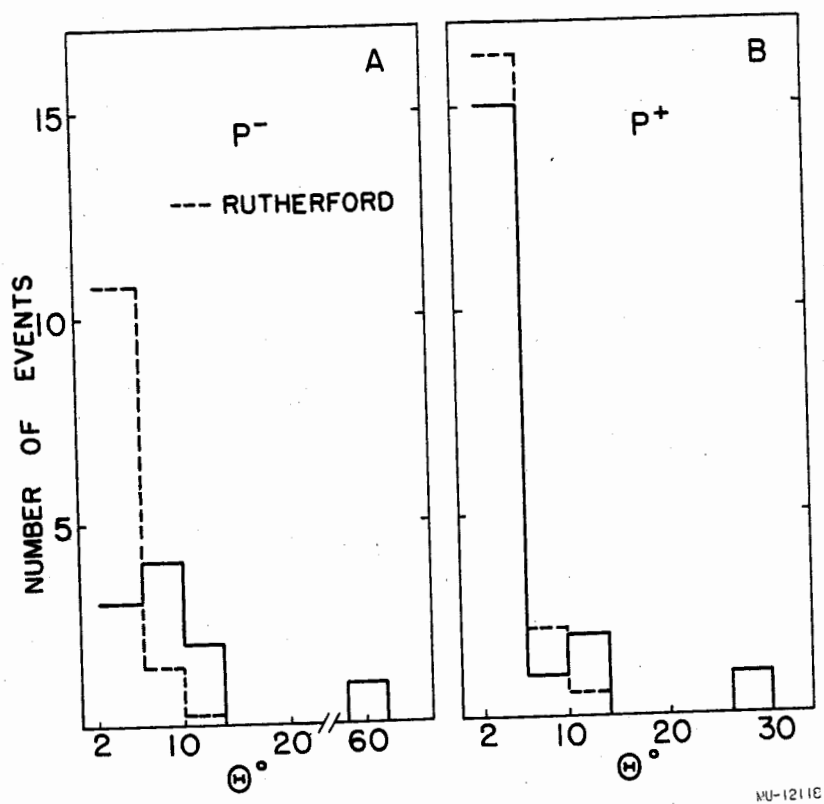
^b $\sigma_0 = \pi (r_0 A^{1/3})^2$ and $r_0 = 1.2 \times 10^{-13}$, $R_{p^-} = r_{p^-} A^{1/3}$.

2. Elastic Scattering

In previous sections we have considered only strong interactions. We have also followed a total path length of 158.3 cm of antiproton track in the energy interval 50 to 200 Mev, paying special attention to small-angle scattering in order to see if we could detect any departure from Rutherford scattering. For comparison, a similar procedure was applied to positive proton tracks.

This section deals therefore with elastic and (or) nearly elastic scatters (i. e., no visible change in grain density and no visible excitation of the struck nucleus). We observed scatters with essentially 100% efficiency for antiprotons of energy 50 Mev or greater, when the horizontally projected angle of scattering was 2° or greater. In the following, we consider only scatters that satisfy the above criteria. The space angle of scattering, θ , has been measured for all such scatters and is shown in Fig. 4A, along with the distribution expected for pure Rutherford scattering. The scanning efficiency and correction factors have been checked by measurements on tracks of 50 positive protons in the energy interval 50 to 100 Mev (Fig. 4B), where it is known that Rutherford scattering predominates below 6° .⁹

⁹K. Strauch, Sixth Annual Rochester Conference, 1956; to be published.



MU-1211C

Fig. 4

The expected number of Coulomb scatters was calculated by (a) assuming the Rutherford (point nucleus) cross section, (b) averaging over the emulsion contents, and (c) multiplying by the efficiency for observing the given interval of space angle. This efficiency is the probability that a given space angle will be associated with a horizontally projected angle of 2° or greater.

For negative protons the grouping of scatterings below 15° indicates diffraction scattering. The expected rise in the 2° -to- 6° interval due to Rutherford scattering appears to be missing, which suggests a possible destructive interference between nuclear and Coulomb scattering. The probability of obtaining three or fewer events when 10.7 are expected is 0.006; however, the possibility of a statistical fluctuation is not excluded. A destructive interference between Coulomb and nuclear scattering does not necessarily imply that the real part of the antiproton-nucleus potential is repulsive. Preliminary calculations indicate that such a destructive interference could be a consequence of the strong absorption of antiprotons by nuclei.

3. The Antiproton Cross Section at Low Velocities

In considering the annihilation of antiprotons with nucleons, it is of interest to know how the cross section for such interactions varies with energy. If the annihilation cross section should increase rapidly with decreasing antiproton velocity,¹⁰ then it would be possible for the antiproton to undergo annihilation, rather than being brought to rest by ionization loss. It is important therefore to establish upper limits to the residual range of antiprotons that are believed to undergo annihilation "at rest". Within the limits of sensitivity of our method ($T_p \leq 0.8$ Mev) we found that all antiprotons were effectively brought to rest.

a. Determination of residual range

In our experiment, 14 examples have been observed in which--judging from the gap density of the track close to the star--the antiproton had a residual range of less than 500 microns.

Scattering measurements were made on these tracks by the constant sagitta method (Gottstein's scheme¹¹) over a distance of 150 microns from the star. The mean sagitta or second difference, \bar{d} , was calculated for each

¹⁰Hans-Peter Duerr and E. Teller, Phys. Rev. 101, 494 (L) (1956). Hans-Peter Duerr, Phys. Rev. 103, 469 (1956).

¹¹Fay, Gottstein, and Hain, Supplemento, Il Nuovo Cimento 11, 234 (1954).

event, and the distribution in \bar{d} for all events is shown in Fig. 5 (A). Figure 5 (B) shows a similar distribution obtained from 20 positive protons coming to rest, Fig. 5 (C) that for 20 protons with a residual range of 100 microns (scattering measurements made from 100 to 250 microns residual range).

The scattering scheme used was such as to give an expected $\bar{d} = 0.51 \pm 0.17$ micron for protons over the range 0 to 150 microns, and $\bar{d} = 0.25 \pm 0.08$ micron over the range interval 100 to 250 microns. The errors refer to standard deviations arising from the finite number of cells (ten) on each track. The mean value of \bar{d} for all antiprotons is 0.50 ± 0.04 micron, whereas that for positive protons is 0.52 ± 0.03 micron. For positive protons with a residual range of 100 microns, $\bar{d} = 0.23 \pm 0.02$ micron. From these figures, and the expected variation of \bar{d} with residual range, we can calculate that the average residual range of the slow antiprotons at annihilation is less than 10 microns ($T_{p^-} \leq 0.8$ Mev).

b. Variation of cross section with velocity

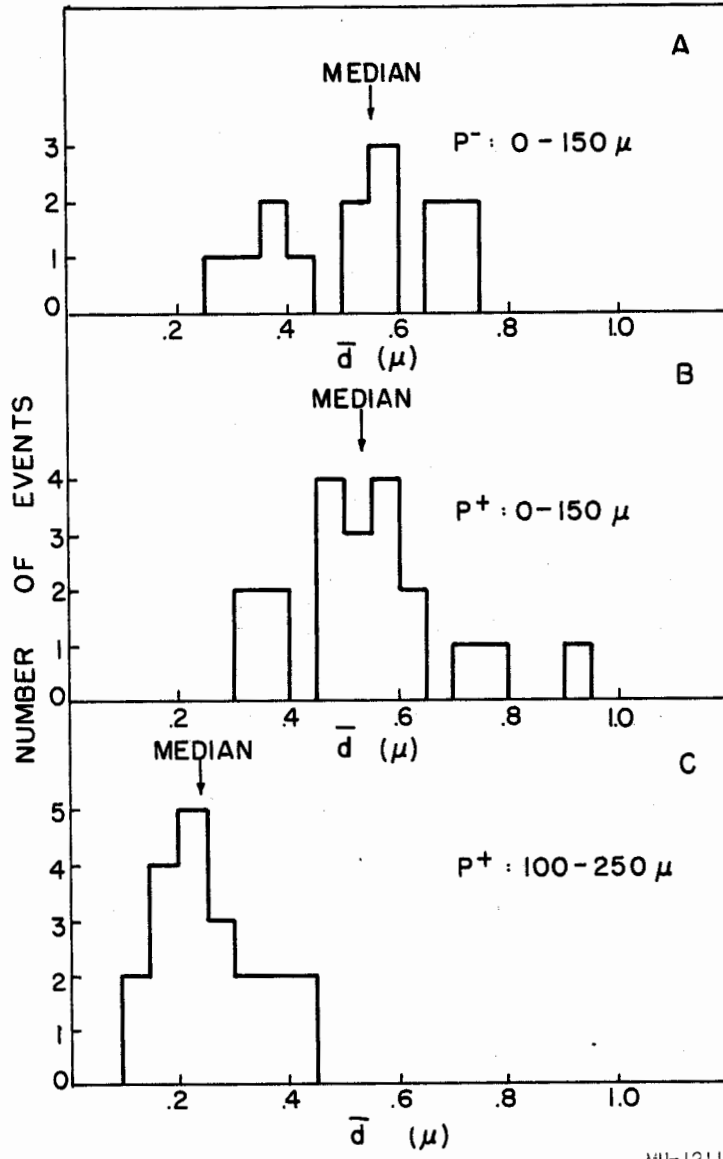
Of the 35 antiprotons observed, 14 survived to the ends of their ranges. At present the statistics are too poor to determine the variation of the annihilation cross section with velocity even over the last centimeter of range, where the variation of velocity with range is most rapid. The very sketchy information available can be considered as follows.

We represent the cross section for annihilation by a power law $\sigma = c \beta^{-m}$. Assuming for simplicity that all antiprotons have the same initial range of 12 cm, we can then calculate by integration the expected number of antiprotons which, having survived 11 cm (or 10 cm), should interact in the last centimeter (or last 2 cm) for any value of m . The results are shown in Table VII.

The results indicate that m is unlikely to exceed unity. These figures do not depend at all critically on the assumed initial range.

Table VII. Number of antiproton interactions for $\sigma = c \beta^{-m}$

Expected number of interactions in residual range	$\sigma = c \beta^{-m}$				Number of p^- interactions observed
	$m = 0$	$1/2$	1	2	
0 to 1 cm	1.2	1.7	2.5	3.3	0
0 to 2 cm	2.4	3.2	4.2	7.7	3



MU-12119

Fig. 5

IV. THE ANTIPROTON ANNIHILATION PROCESS

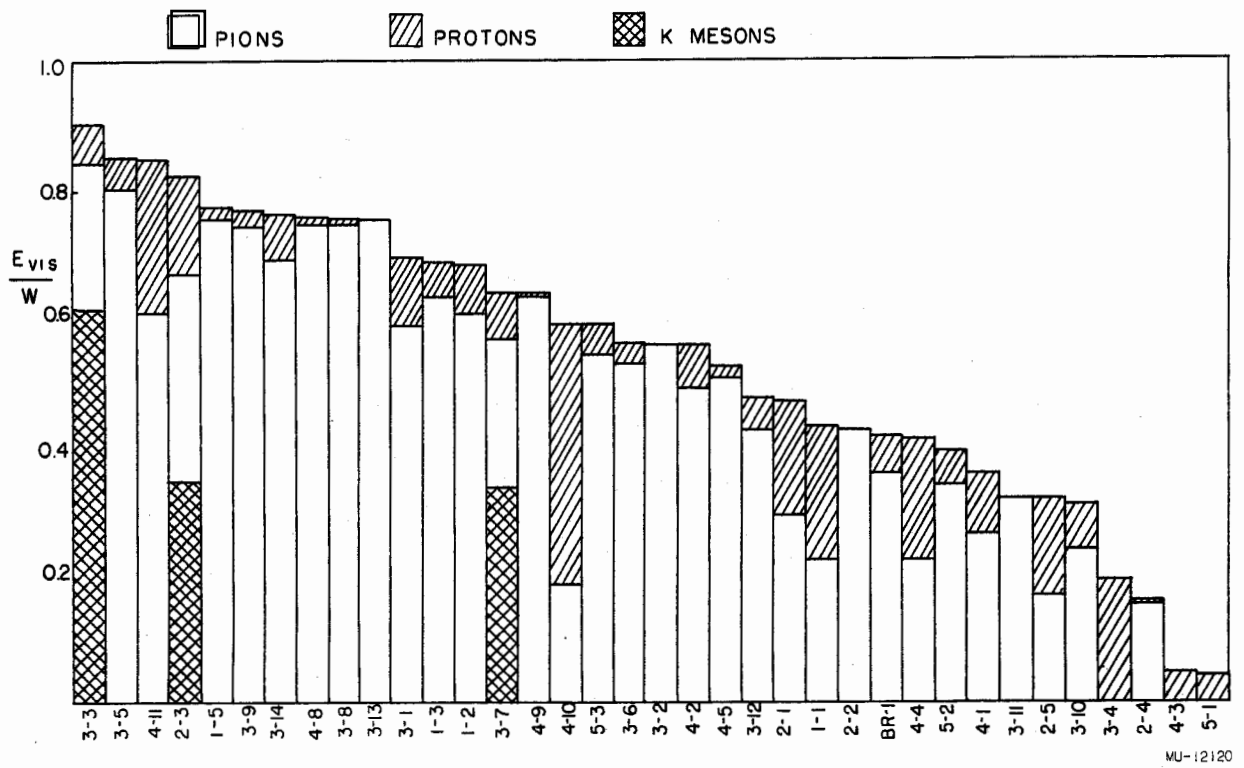
A. The Visible Energy Release in the Annihilation Stars

In this section we discuss the manner in which the energy released in the annihilation process is distributed. Experimentally we observe pion, nucleon, and occasionally K-meson emission. The observed number of charged pions emitted varies from a maximum of five down to zero. In addition to pions, heavy particles are emitted, i. e., protons, alpha particles, and deuterons, whose number (N_H) and energy (E_H) vary over a wide range. The number of charged pions emitted is correlated with the energy in heavy prongs. On the average a star with many pions shows less energy in heavy prongs (Section IV C), and vice versa. It appears that the primary process of the annihilation proceeds predominantly through pion emission while nuclear excitation arises from pion reabsorption and inelastic scattering. Table VIII-a lists the visible energy release, E_{vis} , in all the observed antiproton stars.

E_{vis}/W is shown in Fig. 6 for the 36 individual annihilation stars. It is interesting to note that 21 out of 36 stars have a value of $E_{vis}/W > 0.5$. Table VIII-b lists the total visible energy for stars with evidence for K-meson emission. Each of these stars is described in detail below (Appendices II and III). A few detailed examples of annihilation stars are given in Appendix I.

B. The Pion Spectrum

An attempt was made to obtain the energy of all the observed "shower particles," i. e. particles with less than 1.4 times minimum ionization. In 36 antiproton stars under discussion here, 93 such tracks were observed and their energy measured. Whenever a definite mass identification was possible these particles were found to be pions. We have therefore treated all shower particles as pions in this paper. Table VIII A, columns 8 to 12, lists the pion energies. The energy values were obtained from multiple-scattering measurements. The accuracy to which these energies are known varies considerably depending on dip angle and on the presence of local distortions such as occur at the edge of pellicles. The statistical error of the energy measurements is given. Some pions come to rest. For these the energy is accurately known from the range, and the pion charge is then indicated as π^+ or π^- . For tracks for which conclusive measurements were not possible, only energy estimates (\sim) or lower limits ($>$) are given. To obtain a reliable and unbiased pion spectrum we have first used only pion tracks with dip angle $< 20^\circ$ (shaded region



MU-12120

Fig. 6

Table VIII

A. Data on antiproton annihilation stars

B. Data on antiproton annihilation stars with observed K particles

Column 1 gives the star reference number. The first number refers to the workers by whom the star was found and analyzed, see Section II B.

Column 2 lists the number of charged pions $N_{\pi\pm}$. The stars are grouped in decreasing order of charged pions.

Column 3 lists the number of heavy prongs N_H . In each group the stars are listed in the order of increasing number of heavy prongs.

Columns 4, 5, and 6, respectively, list the total energy per star emitted in charged pions $\Sigma E_{\pi\pm} = \Sigma (T_{\pi\pm} + M_{\pi} c^2)$ and in heavy prongs $\Sigma E_H = \Sigma (T_H + E_B)$, and the total visible energy, $E_{vis} = \Sigma E_{\pi\pm} + \Sigma E_H + \Sigma E_{K\pm}$.

Column 7 gives the kinetic energy of the antiproton T_{p^-} at the interaction. We observed antiproton annihilations in an energy interval from 200 Mev down to 0 Mev (stars at rest). The kinetic energy of the antiproton is small compared with the Q of the annihilation process

$$Q = 2M_p c^2 - E_B = 1876.8 = 1868 \text{ Mev},^{12}$$

where E_B is the binding energy of the nucleon that is being annihilated.

Columns 8 to 12 list the observed pion kinetic energy $T_{\pi\pm}$.

Columns 13 to 15 give the quantities: total energy in charged pions, total energy in heavy prongs and the total visible energy expressed as a fraction of W , the total available energy. Here $W = Q + T_{p^-}$. Such a normalization permits us to consider stars at rest and in flight on an equal footing.

¹²For annihilations at rest when the P^- must be annihilated from a bound atomic orbit, Q is further reduced by this binding energy.

Table VIII A

(1)	(2)	(3)	(4)	(5)	(6)	(7)	(8)	(9)	(10)	(11)	(12)	(13)	(14)	(15)
Star No.	N _π	N _H	Σ E _π	Σ E _H	E _{vis}	T _{p-}	π meson kinetic energies (Mev)					Σ E _π /W	Σ E _H /W	E _{vis} /W
							I	II	III	IV	V			
3-13	5	0	>1415	0	>1415	0	98±40	>100	>100	117±35	>300	0.757	0	0.757
3-8	5	1	1555	14	1569±175	202	75(π ⁺)	115±65	140±18	225±80	300±130	0.751	0.007	0.758
3-1 ^a	5	3	1106	194	1300±50	0	30±6(π ⁺)	34(π ⁻)	43(π ⁻)	125±25	174±40	0.592	0.104	0.696
4-9	4	1	1270	13	1283	140	80±20	130±30	180±40	320±30		0.633	0.006	0.639
3-9	4	1 + 1 rec	1390	48	1438±190	0	95±40	170±45	205±85	360±160		0.744	0.026	0.770
3-6	4	2	~1023	25	~1048	0	78±12	115±15	120±25	~150		0.549	0.013	0.562
4-8 ^b	4	2	1400	19	1419	0	60±5	140±30	220±30	420±70		0.750	0.010	0.760
3-14	4	4	>1428	146	>1574	187	78±15	190±85	>260	~340		0.695	0.071	0.766
1-3	4	5	>1183	102	>1285	0	20(π ⁻)	>115	208±25	280±30		0.633	0.055	0.688
4-11	4	8	>1215	478	>1693	125	60±15	95±20	>100	~400		0.610	0.240	0.850
2-2	3	0 + 1 rec	>792	0	> 792	0	≥120	125±25	127±27			0.424	0	0.424
1-5	3	1	~1420	26	~1446	0	176±30	304±60	~520			0.760	0.014	0.774
4-5	3	2	1040	36	1076	183	50(π ⁻)	170±30	400±40			0.507	0.018	0.525
5-2	3	4	679	100	779	131	59±7	98±25	102±30			0.340	0.050	0.390
1-2	3	4	1135	148	1283	0	125±30	190±45	400±180			0.608	0.079	0.687
3-5	3	5	>1605	99	>1704	132	225±25	>420	~540			0.803	0.050	0.853
4-2	3	5	> 980	134	>1114	130	~100	>160	~300			0.491	0.067	0.558
3-12	3	5	885	103	988±50	205	72±15	93±15	300±40			0.427	0.050	0.477
3-11 ^c	2	0	> 620	0	> 620	80	140±60	>200				0.318	0	0.311
3-2	2	0 + 2 rec	1050	0	1050	0	300±190	470±150				0.562	0	0.562
4-1	2	4	515	165	680	58	60±15	175±70				0.267	0.086	0.353
3-10	2	4	466	131	597±80	77	31±6	155±75				0.240	0.067	0.307
5-3	2	6	> 880	223	>1103	0	>300	>300				0.471	0.119	0.590
2-1	2	7	~ 552	328	~ 880	0	122±20	~150				0.296	0.176	0.472
BR 1 ^d	2	7	670.5	101	771.5	0	57.5±8	332±60				0.360	0.054	0.414
4-4	2	11	445	358	803	90	35(π ⁻)	130±30				0.227	0.183	0.410
1-1	2	13	462	418	880	182	75(π ⁻)	107±30				0.225	0.204	0.429
2-4	1	1	~290	11	~ 301	0	~150					0.155	0.006	0.161
2-5	1	6	315	279	594	0	175±40					0.169	0.149	0.318
4-10 ^e	1	16	380	840	1220	200	240±50					0.184	0.406	0.590
5-1	0	5	0	91	91	150						0	0.045	0.045
4-3	0	5	0	90	90	0						0	0.048	0.048
3-4	0	6 + 1 rec	0	372	372	84						0	0.191	0.191

Table VIII B

(1)	(2)	(3)	(4)	(5)	(6)	(7)	(8)	(9)	(10)	(11)	(12)	(13)	(14)	(15)	(16)	(17)
Star No.	N _K	N _π	N _H	Σ E _K	Σ E _π	Σ E _H	E _{vis}	T _{p-}	K meson kin. energies (Mev)		π meson kin. energies (Mev)		Σ E _K /W	Σ E _π /W	Σ E _H /W	Σ E _{vis} /W
									I	II	I	II				
3-3	2	2	7 + 1 rec	1260	470	127	1857	183	80±8	195±50	90±50	100±50	0.614	0.229	0.062	0.905
3-7	1	2	6	680	467	147	1298	152	187±40		52±13	135±22	0.337	0.231	0.073	0.641
2-3	1	1	3	678	639	300	1617	90	146±37		534±200		0.346	0.327	0.153	0.826

^aFrom Ref. 4.

^bSee Ref. 2.

^cConsistent with P⁻ - H annihilation.

^dFrom Ref. 1.

^eFrom 900 Mev/c exposure, Stack 69.

in Fig. 7). These pion energies are given in bold face letters in Table VIII A. The average pion kinetic energy obtained from the sample of tracks with dip angles $< 20^\circ$ is 170 Mev. We also evaluated the average kinetic energy for all pions irrespective of the dip angle. These include:

- (a) tracks measured by the surface angle or grid coordinate methods (see Appendix IV),
- (b) tracks for which the energy was only estimated,
- (c) tracks for which the lower limit of the energy was taken as the true energy.

The average energy of all tracks is 182 Mev.

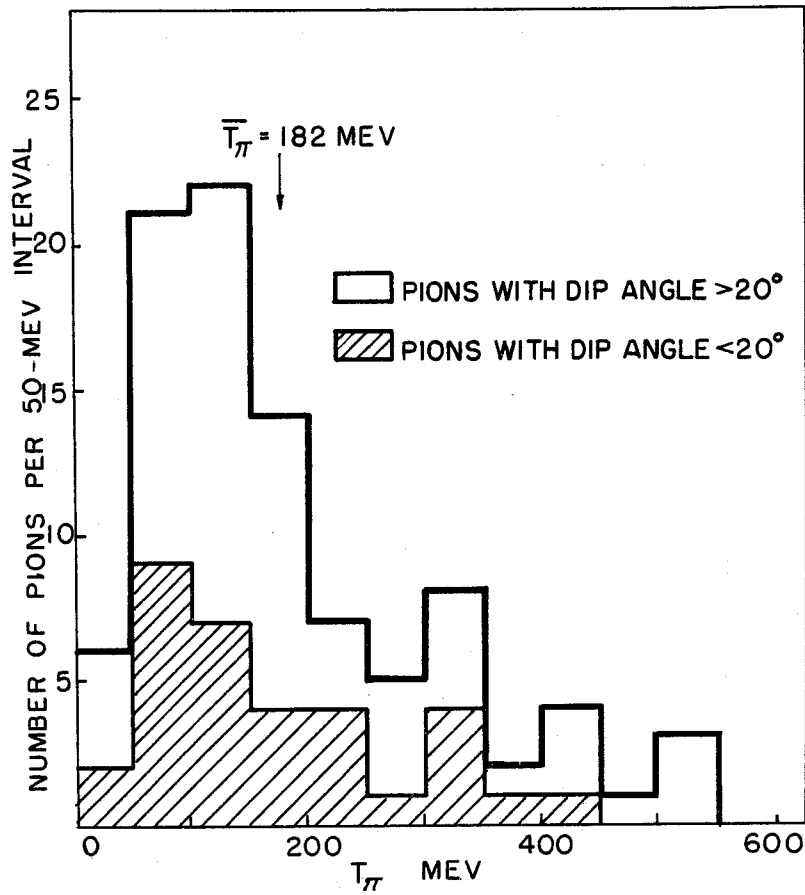
The agreement between the two energy values is good and gives us confidence that even the measurements of tracks under less favorable conditions are satisfactory. In this paper we use the value $\bar{T}_{\pi\pm} = 182 \pm 15$ Mev and $\bar{E}_{\pi\pm} = 322 \pm 15$ Mev as the average kinetic energy and the average total energy, respectively, for charged pions from antiproton annihilation stars. We have evaluated the width of the distribution by computing the root-mean-square deviation of the distribution, and the error on the mean was obtained from this. It must be noted that the observed pion spectrum contains some pions which scattered inelastically in traversing the nucleus. Thus the average observed pion energy ($\bar{E}_{\pi\pm}$) must be lower than the average primary pion energy ($\bar{E}_{\pi\pm}^T$) from the antiproton-nucleon annihilation. We have evaluated the average primary pion energy and have obtained $\bar{E}_{\pi}^T = 346 \pm 20$ Mev. (See Section IV C-3, below).

C. The Nuclear Excitation

1. The energy given to nucleons

The energy transfer to the nucleus can be understood as a secondary phenomenon due to pion absorption and inelastic scattering. Experimentally we observe the energy of charged particles (mainly protons and alpha particles), and must infer from this the total energy transfer, including the energy given to neutrons. The total energy transferred to nucleons is needed for the energy balance in the annihilation process and also for the determination of the number of pions absorbed and inelastically scattered.

To obtain the total energy transfer to nucleons we analyzed the observed proton spectrum (Fig. 8) in terms of a "knock-on" process that gives rise to fast nucleons ($T_p > 35$ Mev), and an evaporation process (for $T_p < 35$ Mev) due to the nuclear excitation of the residual nucleus.



MU-12121

Fig. 7

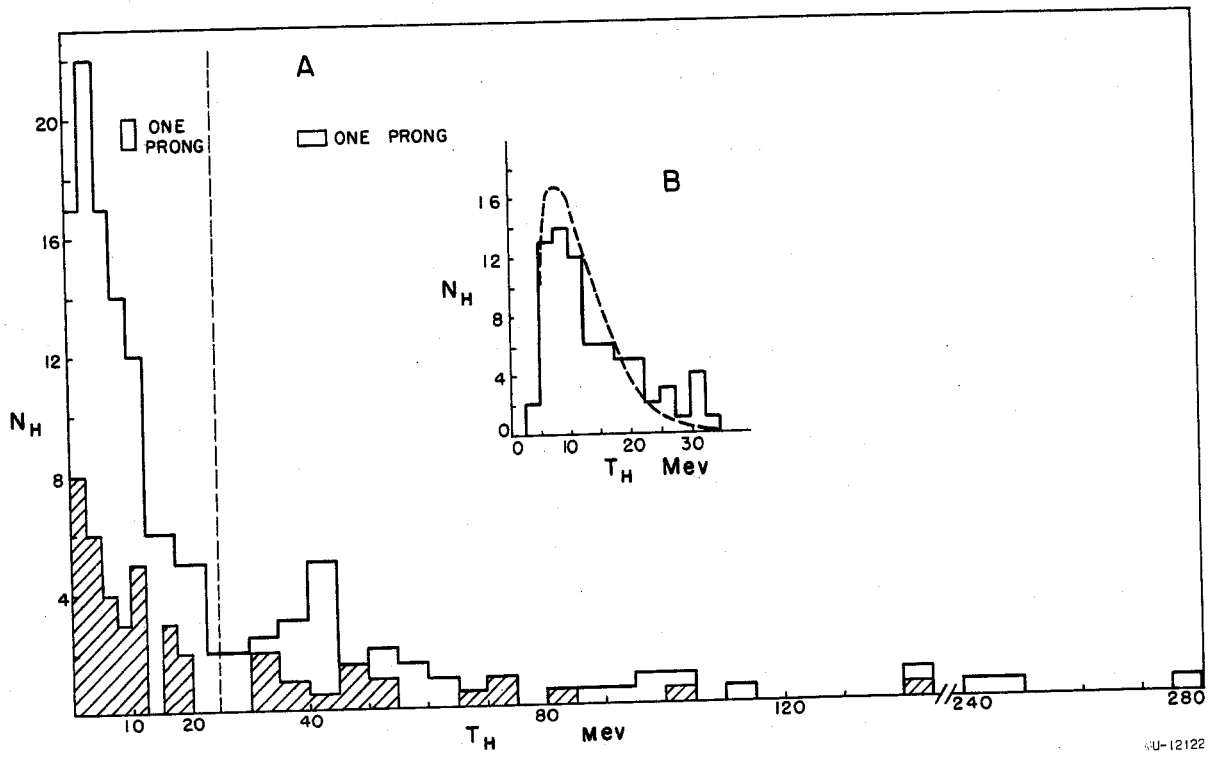


Fig. 8

We have estimated the energy transfer to nucleons corresponding to the knock-on spectrum U_{KO} by measuring the energy of protons greater than 35 Mev, and assuming that the knock-on neutrons have the same energy spectrum as the protons. The ratio of neutrons to protons for the knock-on process has been taken to be $n/p = \langle (A - Z)/A \rangle_{\text{emulsion}} = 1.2$.

The part of the excitation U_{EV} corresponding to the evaporation spectrum has been estimated as follows.¹³ The average evaporation energy in protons per star was obtained from the measured ranges for $T_H < 35$ Mev. To obtain the average evaporation energy in neutrons, a ratio of neutrons to protons $n/p = 4$ was assumed and an average neutron energy equal to 3 Mev was used.¹⁴

Table IX lists the average energy per star in "knock-on" particles U_{KO} , in evaporation particles U_{EV} , and the average total energy per star given to nucleons U , where $U = U_{KO} + U_{EV} = 400 \pm 30$ Mev. The error has been estimated from extreme variations on the above assumptions.

Table IX. The average energy given to nucleons in antiproton annihilation stars. The nuclear excitation U is composed of the energy in evaporation particles U_{EV} and the energy in "knock-on" particles U_{KO} .

Annihilation	U_{KO} (Mev)	U_{EV} (Mev)	U (Mev)
at rest	150	115	265±20
in flight	290	215	505±40
combined	230	170	400±30

¹³ Menon, Muirhead, and Rochat, *Phil. Mag.* 41, 583 (1950); K. J. Le Couteur, *Proc. Phys. Soc. (London)* 63A, 259 (1950). It must be noted that the incomplete identification of the heavy prongs leads to an overestimate of U_{EV} by about 15%. This correction was obtained by comparing the proton and alpha spectra from sigma stars. The values quoted in the text were corrected for this effect.

¹⁴ E. E. Gross, *The Absolute Yield of Low-Energy Neutrons from 190-Mev Proton Bombardment of Gold, Silver, Nickel, Aluminum, and Carbon* (thesis), UCRL-3330, Feb. 1956.

2. Correlation of charged pion multiplicity and energy transfer to nucleons

In Table X we have grouped the annihilation stars according to the number of charged pions observed, $N_{\pi\pm}$. There is a correlation between the number of pions observed and the corresponding average energy in heavy prongs $\Sigma \bar{E}_H$ listed for each group (Col. 2 and Col. 5). A similar correlation can be observed between $N_{\pi\pm}$ and the average number of heavy prongs emitted, \bar{N}_H . On the average a high pion multiplicity is associated with little energy release in heavy prongs and a small \bar{N}_H . In Fig. 9 we have plotted a histogram of the observed energy release in heavy prongs, and have indicated the energy corresponding to absorption of one pion, two pions, and three pions. These data indicate that the mechanism of nuclear excitation goes principally through pion absorption and is thus not a primary phenomenon of the annihilation process. This mechanism is further considered in Section IV G in relation to the consequences of I-spin conservation.

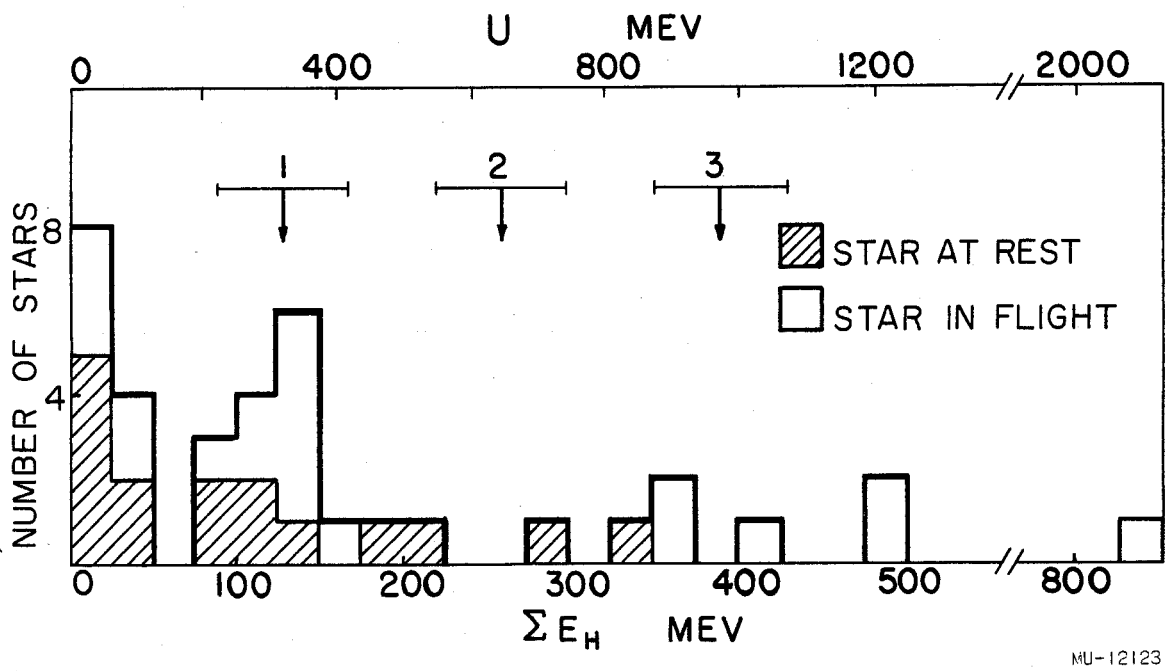
3. Pion interactions

We have shown above that the nuclear excitation can be explained on the basis of nonelastic pion interactions with the nucleus (principally pion absorption). In this section we estimate the average number ν of nonelastic pion interactions per star. To do this, the average energy transfer to the nucleus, U , is equated to the sum of the energy released by pion absorption, $a\nu \bar{E}'_{\pi}$, and inelastic scattering, $b\nu (\bar{T}'_{\pi} - T_0)$. Here ν is the number of pions interacting with the nucleus, a and b are the fractions of these pions absorbed and scattered respectively; hence $a + b = 1$. Further, \bar{T}'_{π} is the average initial kinetic energy of the pion and T_0 is the average final kinetic energy of the inelastically scattered pions. We thus have

$$U = a\nu \bar{E}'_{\pi} + b\nu (\bar{T}'_{\pi} - T_0).$$

Values for b and T_0 are very insensitive to the initial pion energy and can be estimated from other experimental studies of pion interactions in nuclear emulsions.¹⁵ We used the values $b = 0.25$, $T_0 = 40$ Mev, and solved by successive

¹⁵Bernardini, Booth, and Lederman, Phys. Rev. 83, 1277 (1951); G. Goldhaber and S. Goldhaber, Phys. Rev. 91, 467 (1953); S. Goldhaber, Sixth Annual Rochester Conference, 1956 (to be published); Ferretti, Gessaroli, and Stantic, Progress Report No. 1, Physics Dept. University of Bologna, 1956; private communication of G. Puppi; A. H. Morrish, Phys. Rev. 90, 674 (1953); Frank, Gamel, and Watson, Phys. Rev. 101, 892 (1956).



MU-12123

Fig. 9

Table X. Average values of characteristics of antiproton annihilation stars

(1)	(2)	(3)	(4)	(5)	(6)	(7)	(8)
	N_{π^\pm}	\bar{N}_H	$\Sigma \bar{E}_{\pi^\pm}$	$\Sigma \bar{E}_H$	\bar{T}_{π^\pm}	\bar{T}_{p^-}	No. stars
At rest	5	1.5	1261	97	112	0	2
In flight	5	1	1555	14	171	202	1
Combined	5	1.3	1358	38	131	67	3
At rest	4	2.5	1243	49	176	0	4
In flight	4	4.4	1302	212	187	151	3
Combined	4	3.3	1275	119	179	65	7
At rest	3	1.7	1118	58	233	0	3
In flight	3	4.2	1067	94	216	156	5
Combined	3	3.3	1084	81	222	98	8
At rest	2	5	788	163	254	0	4
In flight	2	6.4	493	192	106	118	7
Combined ^a	2	5.9	600	181	160	82	11
At rest	1	3.5	303	145	163	0	2
In flight	1	9.5	510	570	370	144	2
Combined ^b	1	6.5	452	357	266	72	4
At rest	0	5	0	90	-	0	1
In flight	0	5.5	0	233	-	117	2
Combined	0	5.3	0	184	-	78	3
At rest ^c	2.8±0.4	3.1	913±150	106	186	0	16
In flight ^c	2.4±0.4	5.5	763±140	204	178	149	20
Combined ^c	2.6±0.3	4.4	830±110	160	182±15	80	36

^aIncludes 2 stars with K mesons.^bIncludes 1 star with K meson.^cOver-all averages.

approximation for \bar{E}'_{π} and ν . We obtained, for the average primary pion energy, $\bar{E}'_{\pi} = 346 \pm 20$ Mev, and for the average number of nonelastic pion interactions per star, $\nu = 1.3$, giving $a\nu = 1.0$ pion absorbed. (See Table XI for details.)

Table XI. The average number of pions per star, absorbed and inelastically scattered.

	At rest	In flight	Combined
Number absorbed, $a\nu$	0.7	1.3	1.0
Number inelastically scattered, $b\nu$	0.2	0.4	0.3
Number of nonelastic interactions, ν	0.9	1.7	1.3

D. K-Meson Production in Annihilation Stars

In all high-energy interactions in which the energy is above the "K + Hyperon" production threshold, K mesons have been observed. It was therefore expected that K mesons should be produced in nucleon-antinucleon annihilations. Assuming that the conservation of "strangeness"¹⁶ holds for the antiproton annihilation process, one would expect either K- \bar{K} production or K-hyperon production. Only the former is possible for annihilation with a single nucleon, since K-hyperon production requires the presence of an additional nucleon.

In order to find and identify K mesons, all black and grey tracks were carefully examined. The ends of stopping tracks were scrutinized to detect decay products (for K^+) or interactions (for K^-). For tracks not arrested in the stack, mass measurements were carried out whenever possible.

In three of the antiproton stars we have found evidence for charged K-meson emission. In event 3-3 we found evidence for a K- \bar{K} meson pair,

¹⁶M. Gell-Mann, Proceedings of the 1955 Pisa Conference, Nuovo Cimento (to be published).

while in events 3-7 and 2-3 there is evidence for a single charged K meson in each. The detailed measurements on these particles are presented in Appendices II and III.

None of the K particles observed ended within the stack. For the identification we had to rely on ionization and multiple-scattering measurements. Because of possible undetected systematic errors, especially in tracks with large dip angles, the results must be taken with caution. However, in one case (star 3-3, prong 8) the measurements could be performed under favorable conditions. We thus believe that the evidence for a K meson here is conclusive.

E. Angular Distributions of Pions

The angular correlation between charged pions has been measured to obtain further information on the annihilation process.

First, for stars in flight, the forward-backward ratio of pions (in the laboratory system) has been measured, and yields $F/B = 1.4 \pm 0.4$. This is to be compared with a value of $F/B = 1.8$, which has been computed on the assumption that all the pions are created in the primary annihilation process with an isotropic distribution in the center-of-mass system, neglecting pion absorption. The experimental distribution of pion emission as a function of space angle θ (lab), is shown in Fig. 10, together with the theoretical curve for isotropic center-of-mass system distribution averaged over antiproton energy, Fermi momentum of target nucleon, and energy of created pions. Small errors in these parameters have little effect on the expected θ distribution.

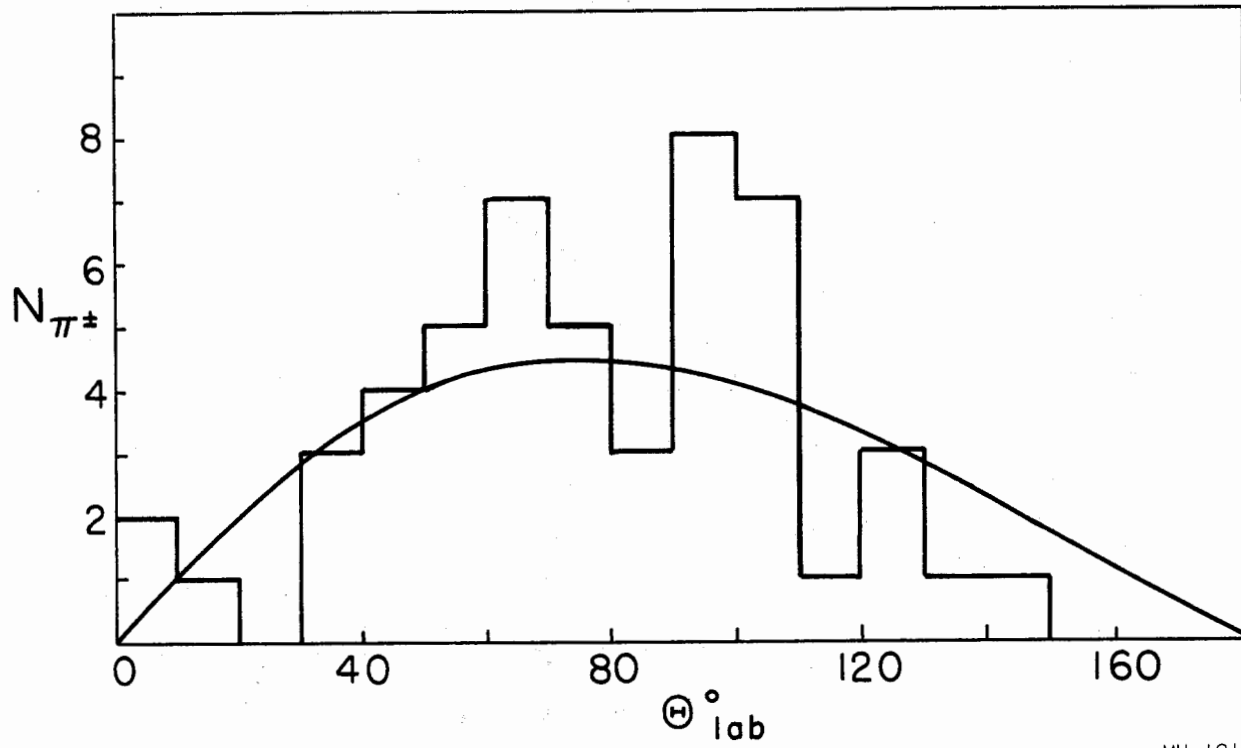
Secondly, the angular correlation between pairs of pions has been measured. The experimental histogram is plotted in Fig. 11. Also shown is the curve expected if the pions are uncorrelated (direction at random). The good agreement between the two makes it unlikely that there is a strong pion-pion interaction that might result in close pairs.

F. Properties of Annihilation Stars

We have summarized the properties of the annihilation stars in Table X. The stars have been grouped according to the number of charged pions observed. In columns 3 to 7 we have listed:

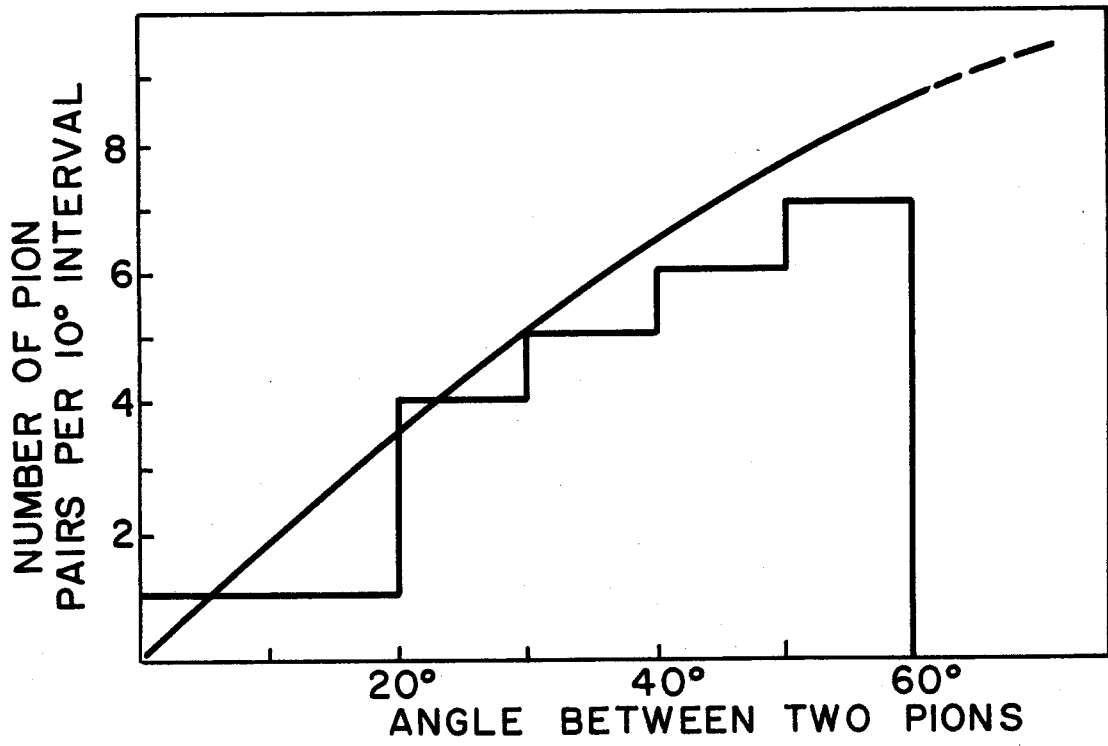
\overline{N}_H , the average number of heavy prongs per star;

$\Sigma \overline{E}_{\pi^\pm}$, the average total energy in charged pions per star;



MU-12124

Fig. 10



MU-12125

Fig. 11

$\Sigma \overline{E}_H$, the average total energy in heavy prongs per star;

$\overline{T}_{\pi\pm}$, the average kinetic energy per pion;

\overline{T}_p , the average antiproton kinetic energy at the interaction.

All the above quantities have been averaged over groups of stars with constant $N_{\pi\pm}$. At the bottom of the table we have listed the averages over all stars. In the following sections we use the information in Table X to carry out an energy balance and to calculate the average pion multiplicity.

1. The energy Balance

We have observed the energy in charged particles emitted from annihilation stars and we want now to infer from the measured quantities the energy given to neutral particles. The energy in neutrons has been included in U , the total energy transferred to nucleons ($U = 400 \pm 30$ Mev, see Section IV C). The energy of K mesons per star has been estimated to be $\Sigma \overline{E}_{K-\overline{K}} = 150 \pm 120$ Mev. In this estimate we considered the conservation of strangeness, the production of neutral $K^0\overline{K}^0$ pairs, and the detection efficiency for K mesons.

We can thus evaluate the average total energy in neutral particles, other than in neutrons and neutral K 's. We have

$$E_{\text{neutral}} = \overline{W} - (\epsilon \Sigma \overline{E}_{\pi\pm} + U + \Sigma \overline{E}_{K\overline{K}}),$$

where \overline{W} ($= 1948$ Mev) is the average total available energy, ϵ ($= 1.1 \pm 0.07$) is the estimated correction for pion detection efficiency, and $\Sigma \overline{E}_{\pi\pm}$ ($= 830 \pm 110$ Mev) is the average pion energy per star as given in Table X. Substituting the numerical values in the equation above, we obtain for the average energy in neutral particles $E_{\text{neutral}} = 485 \pm 170$ Mev.

If we assume that all this energy goes into neutral pions we obtain for the ratio of the energy in charged to neutral pions $\epsilon \Sigma \overline{E}_{\pi\pm} / E_{\text{neutral}} = 913/485 \approx 2/1$, a value consistent with charge independence. Conversely, if we assume that charge independence must hold for the annihilation process, all the available energy is accounted for and there is very little energy available for any other type of neutral radiation (within our present limit of errors).

The results of this section are summarized in Table XII. We also list in the table the corresponding values for interactions in flight and at rest separately.

Table XII. Energy balance in average antiproton annihilation star

	At rest (Mev)	In flight (Mev)	Combined (Mev)
$\epsilon \Sigma \bar{E}_{\pi^{\pm}}$	1005±170	840±150	913±120
U	265±20	505±40	400±30
$\Sigma \bar{E}_{K\bar{K}}$	150±120	150±120	120±120
E_{neutral}	448±200	522±200	485±170
\bar{W}	1868	2017	1948

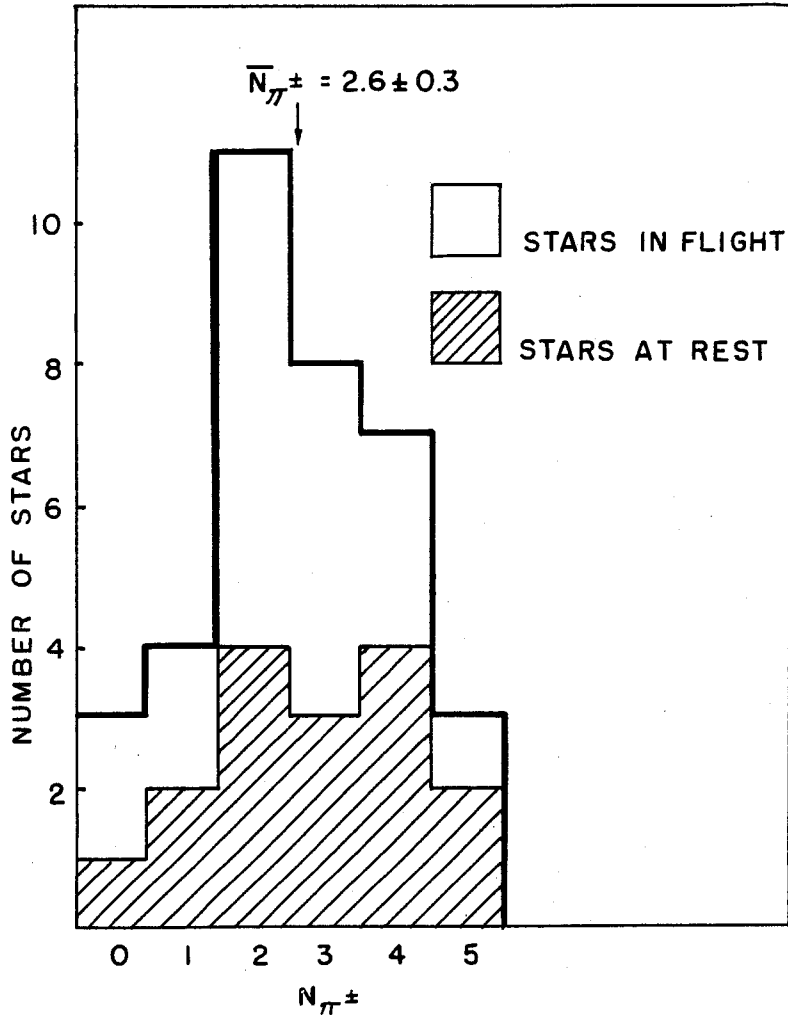
2. The Average Pion Multiplicity

In this section we estimate the average pion multiplicity \bar{N}_{π} in the annihilation process. This estimate can be carried out by two independent methods. Method (a) employs the average number of charged pions emitted, and assumes that the number of neutral pions is equal to one-half the number of charged pions produced. Method (b) uses the average charged pion energy and assumes that the average neutral pion energy is the same as the average charged pion energy. The assumptions mentioned are consequences of charge independence. The results of these two methods agree very closely, and when combined give $\bar{N}_{\pi} = 5.3 \pm 0.4$.

Method (a). The distribution of the observed charged-pion multiplicity $N_{\pi^{\pm}}$ is plotted in Fig. 12. The average value of the observed pion multiplicity for all stars is $\bar{N}_{\pi^{\pm}} = 2.6 \pm 0.3$. This value, when corrected by the efficiency factor $\epsilon = 1.1 \pm 0.07$, can be used to obtain an estimate of the lower limit to the average pion multiplicity \bar{N}_{π} . Assuming charge independence, we get

$$\underline{\lim} \bar{N}_{\pi} = 3/2 \epsilon \bar{N}_{\pi^{\pm}} = 4.3 \pm 0.6 .$$

To get the value of \bar{N}_{π} from this lower limit we must add the average number of pions absorbed. This number was shown to be 1.0 in Section IV C-3, giving a value for the average pion multiplicity of $\bar{N}_{\pi} = 5.3 \pm 0.6$. Another estimate of \bar{N}_{π} can be obtained from the group of 12 stars (Fig. 9) with very low visible energy in heavy prongs ($\Sigma E_{\text{H}} < 50$ Mev). If we assume that these stars correspond to no pion absorption, the average multiplicity of charged pions,



MU-12126

Fig. 12

which is 3.3 ± 0.5 for these stars, can be used directly to obtain \overline{N}_π , viz.

$$\overline{N}_\pi = (3/2)(1.1 \pm 0.07)(3.3 \pm 0.5) = 5.4 \pm 0.8 .$$

Method (b). An upper limit for the charged-pion multiplicity is obtained by use of the observed average pion energy $\overline{E}_{\pi^\pm} = 322 \pm 15$ Mev. If we assume that the neutral pions have the same energy spectrum as the charged pions, then from energy considerations we get

$$\overline{\text{lim}} \overline{N}_\pi = \overline{W}/\overline{E}_{\pi^\pm} = 1948/(322 \pm 15) = 6.1 \pm 0.3 .$$

To get the value of the pion multiplicity from this upper limit we must use the primary average pion energy $E'_{\pi^\pm} = 346 \pm 20$ Mev (Sec. IV B) instead of the observed one. In addition we must take into account the energy going into $\overline{K\overline{K}}$ pair production, $\Sigma \overline{E}_{\overline{K\overline{K}}} = 150 \pm 120$ Mev, and subtract this amount from the total available energy \overline{W} . We thus obtain

$$\overline{N}_\pi = (\overline{W} - \Sigma \overline{E}_{\overline{K\overline{K}}})/\Sigma E'_{\pi^\pm} = 5.2 \pm 0.5 .$$

G. Comparison with Statistical Theories

In this section we compare the observed pion multiplicity with that predicted by two statistical models, the Fermi model¹⁷ and the Lepore-Neuman model.¹⁸ For the Fermi statistical model we also compute the probability for \overline{K} -meson production. In addition we compare the observed pion energy spectrum with that derived from phase-space considerations. Finally, we examine the consequences of I-spin conservation as it applies to the charged-pion multiplicity distribution and to the correlation between nuclear excitation and charged-pion multiplicity.

¹⁷E. Fermi, Progr. Theoret. Phys. (Japan) 5, 570 (1950). Application to the annihilation process. R. Gatto, Nuovo Cimento 3, 468 (1956). G. Sudarshan, Phys. Rev. 103, 777 (1956). We found that in this paper the factor $(.945 \frac{\Omega}{\Omega_0})^{N-1}$ occurring in formula (4) is in error and should read $(5.2 \frac{\Omega}{\Omega_0})^{N-1}$ and consequently the calculations presented were actually made for an interaction volume of $(.19) \frac{4}{3} \pi (\frac{\hbar}{m_\pi c})^3$. S. Belenky, V. Maximenko, A. Nikishov, and I. Rosental, Paper presented at Moscow Conference on High Energy Physics, May 1956.

¹⁸J. V. Lepore and M. Neuman, Phys. Rev. 98, 1484 (1955).

1. The Fermi Statistical Model

Disregarding conservation of angular momentum and K meson production, one can write the probability of annihilation into N pions as

$$P_N = \text{const. } S_N T_N (\Omega/6\pi^2)^{N-1} \int \prod_{i=1}^N d^3 p_i \delta(W - \sum_i \epsilon_i) \delta(\sum_i \vec{p}_i),$$

where \vec{p}_i is the momentum of the *i*th particle in units of $m_\pi c$; W and ϵ_i are the total energy and energy of the *i*th particle in units of $m_\pi c^2$; and Ω is the interaction volume in units of $(4/3)\pi (\hbar/m_\pi c)^3$. S_N is a factor taking the indistinguishability of pions into account, and T_N is an I-spin weight factor.

Lepore and Stuart¹⁹ have developed a general method for the evaluation of the integral occurring in P_N . However, for the relativistic case of high multiplicity, the computation is excessively tedious. Fialho²⁰ has evaluated the Lepore-Stuart method in the relativistic case by means of a saddle-point approximation. Although the saddle-point approximation is strictly valid only for high multiplicities, Fialho has studied and determined the corrections necessary for small multiplicities. We have applied the saddle-point approximation to annihilation of antiprotons into pions, and the results are shown in Table XIII.

Thus we find that for an interaction volume of about 10 to 15 Ω_0 , which corresponds to an interaction radius of about $2.3 \hbar/m_\pi c$, the Fermi statistical theory agrees with the observed pion multiplicities, if K-meson production is neglected.

We have also evaluated the relative probabilities according to the Fermi model including K-meson production. For this we have assumed conservation of strangeness i. e. $K\bar{K}$ meson pair production, isotopic spin $I = 1/2$ and spin $S = 0$. The results are shown in Table XIV. Here again we find reasonable agreement with experiment for interaction volumes of about 15 Ω_0 .

2. The Pion Energy Distribution

The pure phase-space energy distribution has been computed by means of the expression

¹⁹J. V. Lepore and R. Stuart, Phys. Rev. 94, 1724 (1954).

²⁰Gabriel E. A. Fialho, Thesis, Columbia University, Nevis Report 22, Feb. 1956.

Table XIII. Distribution of pion multiplicities, according to Fermi model, for different interaction volumes (production of K mesons neglected)

N_π	Probability for annihilation into N_π pions (%)		
	$\Omega = 1$	$\Omega = 10$	$\Omega = 15$
2	6.4	0.1	0.0
3	63.7	5.6	2.3
4	24.6	21.7	13.4
5	5.0	44.0	40.6
6	0.3	23.7	33.1
7	0.0	5.1	10.6
Average No. of pions \bar{N}_π	3.3	5.0	5.4

Table XIV. Distribution of pion and K-meson multiplicities according to Fermi model, for different interaction volumes

N_K	N_π	Probability for annihilation into N_π pions and N_K K mesons (%)		
		$\Omega = 1$	$\Omega = 10$	$\Omega = 15$
0	2	3.8	0.0	0.0
	3	37.2	4.6	2.0
	4	14.4	17.9	11.8
	5	3.3	36.1	35.7
	6	0.2	19.5	28.9
	7	0.0	4.2	9.2
	2	0	5.9	0.0
1		26.6	3.3	1.4
2		8.3	10.2	6.8
3		0.3	4.1	4.1
4		0.0	0.0	0.0
Average No. of pions \bar{N}_π		2.4	4.5	5.0
Probability of producing a K meson pair		41.1%	17.6%	12.3%

$$P(\epsilon) = \text{const.} \frac{dW_{N-1}}{dW_N} \sqrt{\epsilon^2 - m_\pi^2 c^4} \epsilon \int \prod_{i=1}^{N-1} d^3 p_i \delta(W_{N-1} - \sum_{i=1}^{N-1} \epsilon_i) \delta(\sum_{i=1}^{N-1} \vec{j}_i),$$

where W_N is the total annihilation energy shared by N pions and W_{N-1} is the total energy shared by $N-1$ pions in their rest-mass system. The integral has been evaluated by the saddle-point approximation method mentioned above. The above formula would give the exact phase-space distribution if the annihilation proceeded only into pions. Because K mesons are produced in only a small fraction of the stars this is a good approximation to the actual phase-space distributions.

The normalized pion energy spectrum for multiplicities 4, 5, 6, and 7 is plotted in Fig. 13. It has been pointed out that approximately 5% of the experimentally observed pions are expected to have lost energy by inelastic scattering. Therefore, the plotted curves should be slightly depressed at high energies and raised at low energies to make a direct comparison with the experimental spectrum. It is clear, however, that a good fit may be obtained with contributions from a small region of multiplicities near five and six pions.

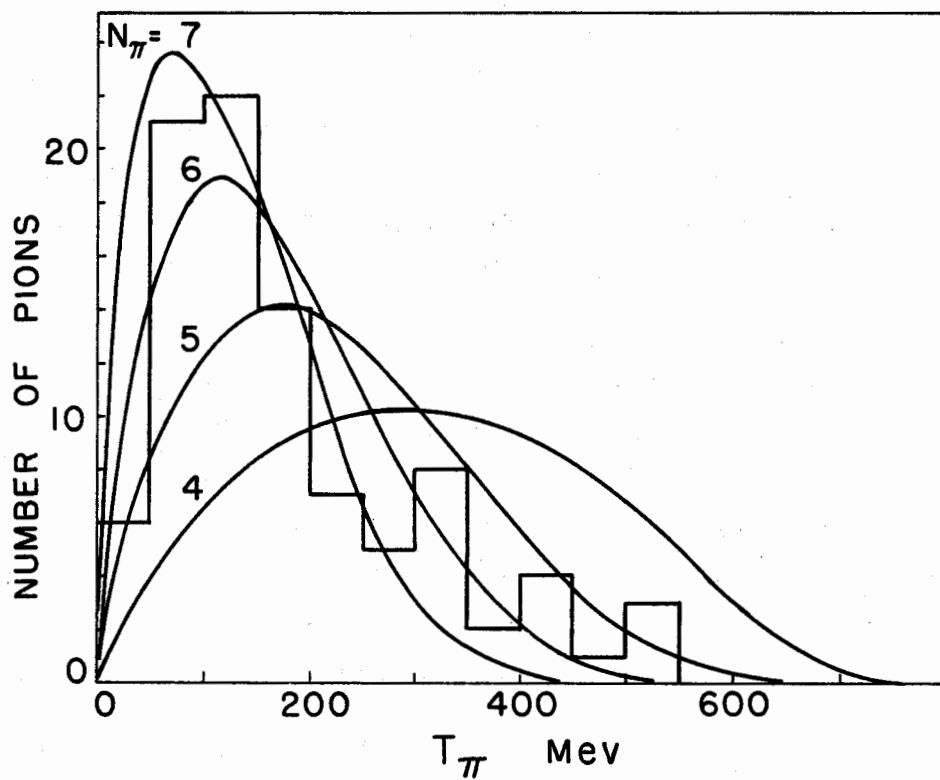
3. The Lepore-Neuman Statistical Model

This model replaces the fixed-volume cutoff of the Fermi model by a gaussian spatial term that is energy-dependent: $\exp(-\chi_i^2 \epsilon_i^2 \tau_i / \hbar^2 c^2)$, where the τ_i are scaling factors characterizing each type of particle in the final state. In addition the Lepore-Neuman model provides for the conservation of the center of energy by means of a term $\delta(\sum_i \chi_i \vec{\epsilon}_i)$. It is shown in Appendix V that the probability of annihilation into N pions may be represented by

$$P_N = \text{const} S_N T_N (2W \sqrt{\pi \tau_\pi})^{-3(N-1)} N^{3N-3/2} \int \prod_{i=1}^N d^3 p_i \delta(W - \sum_i \epsilon_i) \delta(\sum_i \vec{p}_i).$$

The integral may be evaluated as mentioned above. Here again K -meson production was neglected. The results are shown in Table XV for several values of the effective volume parameter, $\tau_\pi^{-3/2}$. Thus we find that for an effective volume parameter $\tau_\pi^{-3/2} \approx 10$ the Lepore-Neuman statistical model agrees with the observed pion multiplicities if K -meson production is neglected. It has been shown by Holland²¹ that effective volume parameters of this order of magnitude can be used to fit pion production in nucleon-nucleon collisions.

²¹D. Holland (Radiation Laboratory, University of California), private communication.



MU-12127

Fig. 13

Table XV. Distribution of pion multiplicities, according to Lepore-Neuman model, for various choices of the effective volume parameter $\tau_\pi^{-3/2}$ (K-meson production neglected)

Probability for annihilation into N_π pions (%)		
N_π	$\tau_\pi^{-3/2} = 1$	$\tau_\pi^{-3/2} = 10$
2	49.4	1.9
3	44.6	17.1
4	5.2	20.0
5	0.8	28.8
6	0.0	21.4
7	0.0	10.8
Average No. of pions \bar{N}_π	2.6	4.8

4. Consequences of I-Spin Conservation

The probability of a given proportion of π^+ , π^0 , and π^- in an annihilation giving N_π pions is determined, through I-spin conservation, by the initial-state total I spin and projection (I, M_I). The annihilation of an antiproton and proton may occur in either the state $(0, 0)$ or the state $(1, 0)$. The annihilation of an antiproton and neutron occurs only in the state $(1, -1)$. Since we are concerned here with annihilations that occur in emulsion ($n/p = 1.2$), we have weighted the initial states according to $(1.0/2.2)[(0, 0)/2 + (1, 0)/2] + (1.2/2.2)(1, -1)$. The results given in Table XVI are the probabilities of creation of a given number of charged pions in an annihilation of given multiplicity. We have neglected K-meson production in these considerations.

We have shown in Section IV C-3 that about 20% of all pions created in the annihilation process are subsequently absorbed by the nucleus. Using this value for the probability of absorption, we have calculated the probability that if a given number of charged pions, N_{π^\pm} , are created in the annihilation, a number $(0, 1 \cdots N_{\pi^\pm})$ emerge. This result has been combined with Table

Table XVI. Probability that a given number of charged pions $N_{\pi\pm}$ are created in an annihilation of given multiplicity, N_{π} .

$N_{\pi\pm}$	N_{π}					
	2	3	4	5	6	7
0	0.076	0.045	0.015	0.006	0.002	0.001
1	0.379	0.218	0.109	0.047	0.020	0.008
2	0.545	0.419	0.258	0.154	0.080	0.039
3		0.327	0.436	0.342	0.234	0.138
4			0.182	0.295	0.289	0.228
5				0.156	0.292	0.330
6					0.084	0.186
7						0.070
$N_{\pi}/\overline{N}_{\pi\pm}$	1.53	1.49	1.50	1.50	1.50	1.50

XVI to determine the probability that $N_{\pi\pm}$ charged pions emerge after an annihilation of multiplicity N_{π} . We have tabulated in Table XVII the number of cases in a total of 33 annihilations (the number we have observed, excluding those with probable K mesons) in which $N_{\pi\pm}$ charged pions emerge for a given multiplicity N_{π} .

It is seen that good agreement may be found by combining a narrow group of multiplicities near $N = 5$.

A correlation is expected between the number of charged pions emerging and the nuclear excitation. Although there is a broad distribution in number of charged pions at annihilation, the probability that charged pion absorption has occurred is greater for stars with a small number of emerging charged pions than for those with a large number. We have used the foregoing results and the probability of absorption and inelastic pion scattering determined in Section IV C to compute the average visible excitation energy as a function of the number of charged pions emerging, $N_{\pi\pm}$, for given multiplicities N_{π} . The results are shown in Table XVIII. The experimental values have large uncertainties because of the small number of cases and because of the broad spread of excitation energies for each $N_{\pi\pm}$. However, the predicted increase in excitation for stars with small numbers of charged pions emerging is evident.

Table XVII. Numbers of cases in a total of 33 in which $N_{\pi\pm}$ charged pions emerge for a given multiplicity N_{π}

Number of charged pions, $N_{\pi\pm}$	Number of cases found experimentally ^a	Calculated number of cases for multiplicity N_{π}					
		2	3	4	5	6	7
0	3	5.9	3.7	1.7	0.9	0.4	0.2
1	3	16.0	11.3	7.3	4.3	2.5	1.4
2	9	11.5	12.9	12.7	9.5	6.8	4.5
3	8		5.5	9.8	10.9	10.2	8.2
4	7			2.4	6.7	8.5	9.4
5	3				1.7	4.2	6.5
6	0					0.7	2.4
7	0						0.5

^aIt must be noted that because of the 90% efficiency for finding minimum secondaries, the experimental distribution is modified from the true distribution.

Table XVIII. Average nuclear excitation, ΣE_H , in charged prongs

$N_{\pi\pm}$	Experimentally found values		Calculated values for multiplicity N_{π}					
	ΣE_H (Mev)	Number of stars	2	3	4	5	6	7
0	184	3	129	168	224	282	330	370
1	357	4	70	121	150	244	289	343
2	181	11	7	68	129	180	238	294
3	81	8		10	64	127	209	242
4	119	7			14	61	134	194
5	38	3				17	73	132
6		0					20	85
7		0						24

H. Discussion on the Annihilation Radius

A comparison between the average pion multiplicity ($\bar{N}_\pi = 5.3$) and the number of pions absorbed and inelastically scattered ($\nu = 1.3$) permits us to estimate the solid angle subtended by the nucleus at the region of annihilation. Although such an argument is qualitative in nature, it gives a measure of the average distance from the center of the nucleus at which the annihilation occurs. Furthermore we note, by a separate analysis of stars at rest and in flight, a difference in the ratio of ν/\bar{N}_π indicating a difference in the average radius (from the center of the nucleus) at which the respective annihilations take place.

Qualitatively, we may discuss these phenomena as follows. In the stars at rest we find a ratio of $(\nu/\bar{N}_\pi)_{\text{rest}} = 0.17$, while for stars in flight this ratio is $(\nu/\bar{N}_\pi)_{\text{flight}} = 0.33$. This difference can be understood by the following argument. For stars at rest the antiproton is captured into Bohr orbits around the nucleus and cascades down until it finds itself in an orbit from which it can annihilate with a nucleon. These orbits are expected to have rather high angular momentum at first, and thus for a large antiproton-nucleon annihilation cross section the overlap between the antiproton wave function and the nucleus causes the annihilation to take place at the surface of the nucleus in the region of reduced nuclear density.⁵ These considerations can explain the small pion absorption mentioned above. On the other hand, for interactions in flight, the antiproton can occasionally penetrate to smaller radii in traversing a mean free path in nuclear matter. The experiment indicates that for annihilations in flight about two pions interact with the nucleus, on the average, as compared with one pion for antiprotons "at rest." This result permits us to estimate a mean penetration depth of antiprotons at high velocity into nuclear matter of the order of 3×10^{24} nucleons/cm², which corresponds to a mean life of 2×10^{-24} sec for antiprotons in nuclear matter. This picture is supported by the fact that the six stars with the highest energy in heavy prongs ($\Sigma E_H > 350$ Mev) all occur in flight. These stars can be considered as examples of head-on collisions in which the antiproton penetrated far enough into the nucleus so that several of the pions produced in the annihilation process were absorbed by the nucleus.

V. ACKNOWLEDGMENTS

The successful exposure of the emulsions used in this experiment was due in part to the help and encouragement of Drs. Owen Chamberlain, Edward J. Lofgren, and Clyde Wiegand. We wish to take this opportunity of expressing our appreciation for their contributions to this work.

We wish to thank the Bevatron crew for their assistance in carrying out this exposure. We also wish to thank Dr. Tom Ypsilantis and Dr. Herbert M. Steiner for their help with the experimental setup and Drs. Dan H. Holland, Robert Karplus, and Joseph V. Lepore for many helpful discussions on this paper. Thirty scanners, some in Berkeley and some in Rome, spent long tedious hours locating the negative protons discussed in this paper. Without their conscientious and tireless efforts this work would not have been possible.

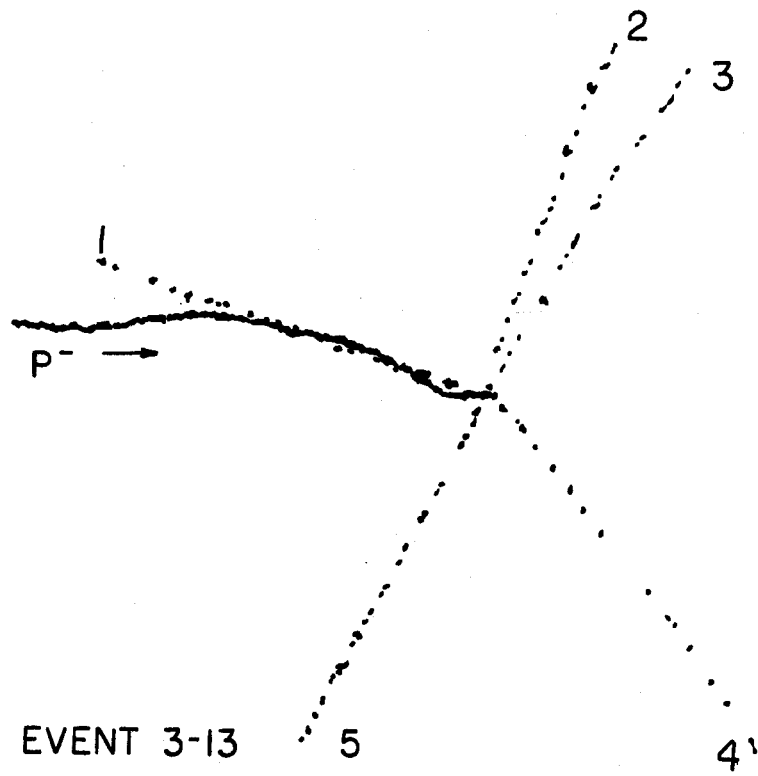
APPENDIX

I. Examples of Antiproton Annihilation Stars

Here we present eight projection drawings of annihilation stars (Figs. A. 1 - A. 8). These include one example for each value of the charged-pion multiplicity, one example of the inelastic scattering of an antiproton, and one of a possible charge-exchange scatter. For each case a table describing the results of the measurements on the individual prongs is given (Tables A. I through A. VIII). For each prong the identity, the projected angle, the dip angle, and the energy E are listed. For pions the energy is given by $E_{\pi} = T_{\pi} + M_{\pi}c^2$, while for protons and α particles it is $E_H = T_H + E_B$, where E_B is the binding energy (8 Mev for protons and 4 Mev for α particles).

Table A. I. Characteristics of the tracks in Event 3-13:
annihilation at rest, giving five charged pions

Track	Type	Projected angle (degrees)	Dip angle (degrees)	E (Mev)
1	π	351	+ 20	238±40
2	π	260	+ 32	257±35
3	π	260	- 36	>440
4	π	134	- 24	>240
5	π	67	+ 39	>240

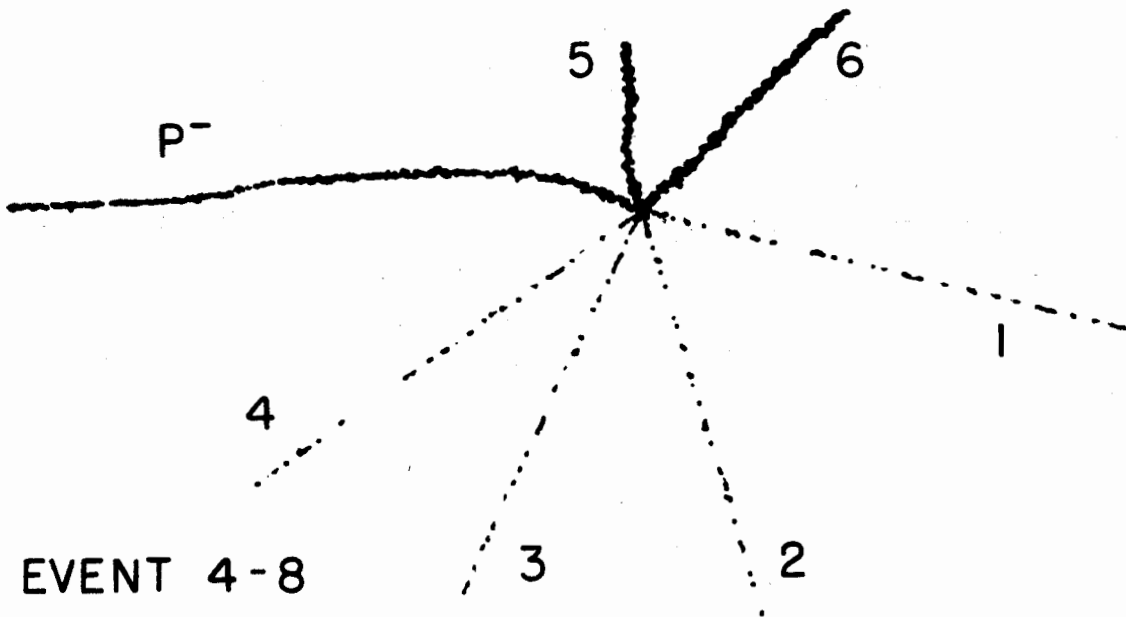


MU-12128

Fig. A.1

Table A. II. Characteristics of the tracks in Event 4-8:
annihilation at rest, giving four charged pions

Track	Type	Projected angle (degrees)	Dip angle (degrees)	E (Mev)
1	π	25.5	+ 4.8	560±70
2	π	308	- 0.7	280±30
3	π	242	- 6.1	200±5
4	π	214	+18	360±30
5	p	134	0	9
6	p	70	+56	10



MU-12129

Fig. A.2

Table A.III. Characteristics of tracks from Event 1-2:
annihilation at rest, giving three charged pions

Track	Type	Projected angle (degrees)	Dip angle (degrees)	E (Mev)
1	p	194	- 60	41.8
2	π	244	+ 50	540 \pm 180
3	π	27	- 42	263 \pm 30
4	p	47	+ 43	55.5
5	π	66	- 17	330
6	p	119	- 21	38
7	p	164	+ 44	11.9

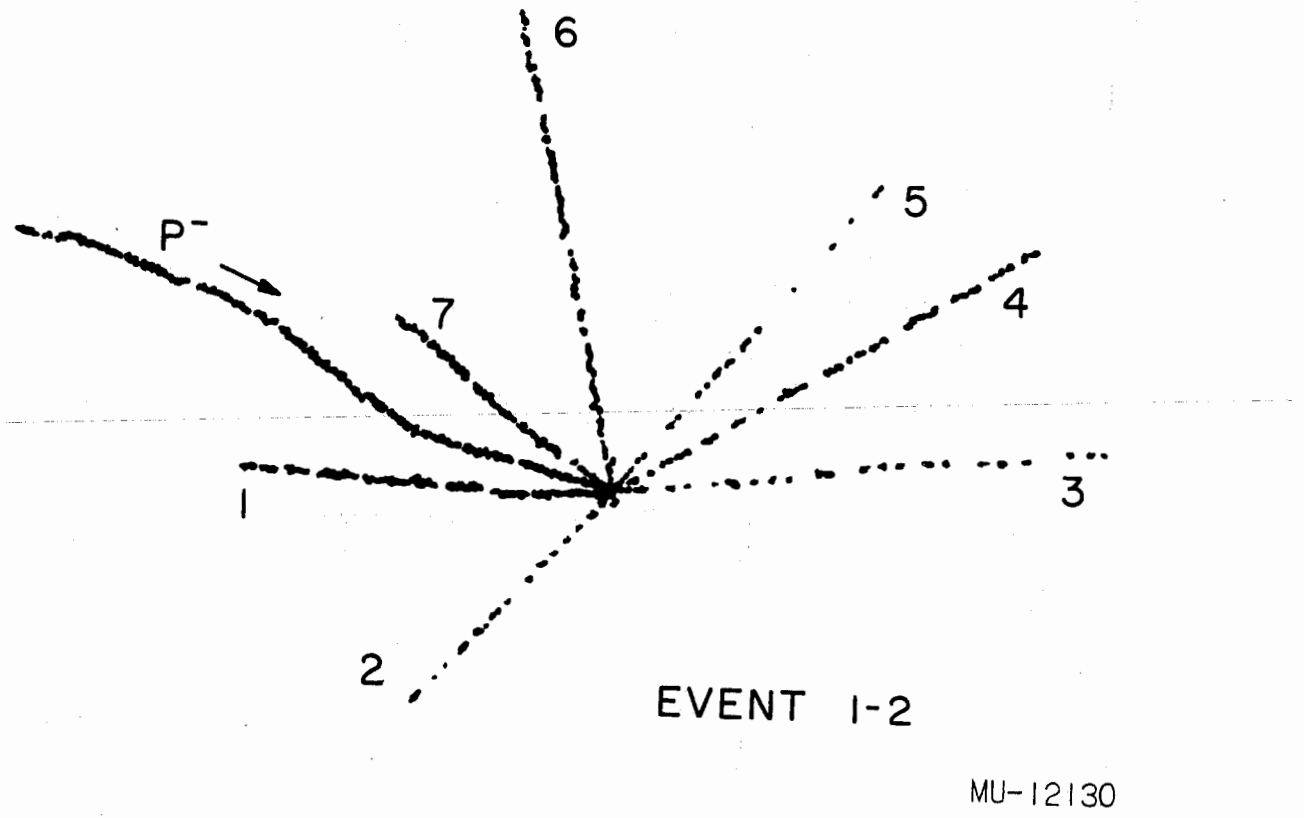


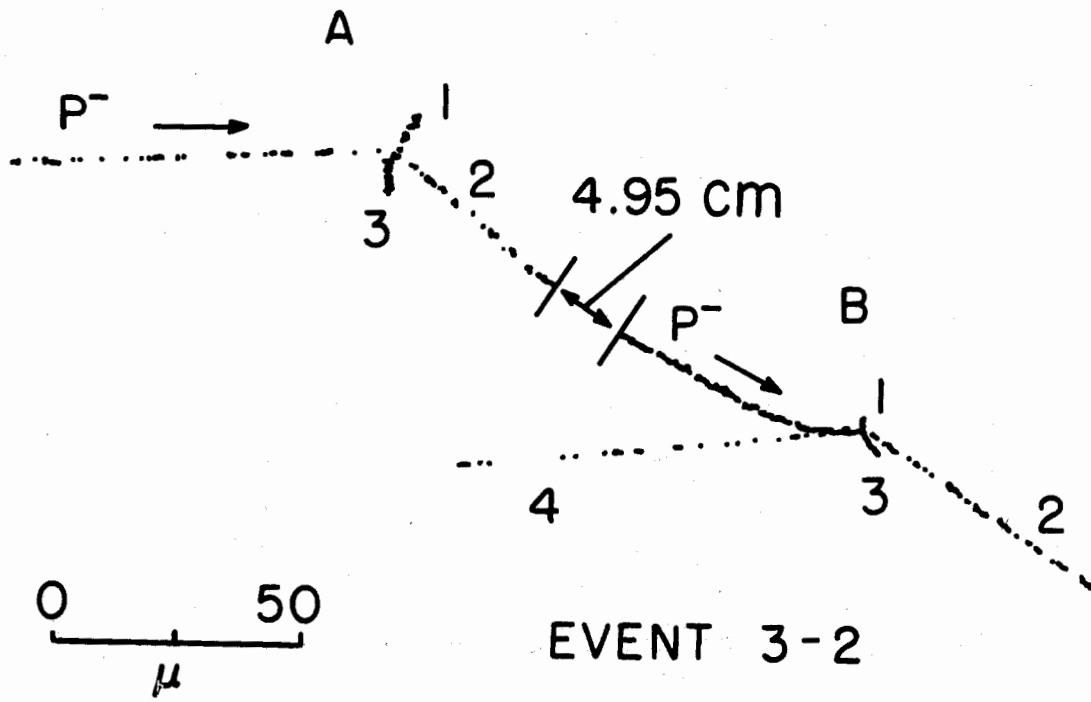
Fig. A.3

Table A.IV. Characteristics of tracks from Event 3-2:

Star A, inelastic scatter, no charged pions;

Star B, annihilation at rest, giving two charged pions

Track	Type	Projected angle (degrees)	Dip angle (degrees)	E (Mev)
<u>Star A</u>				
1	p ⁺	+ 59	~ 0	8.6
2	p ⁻	- 42	-25	
3	α	-104	+73	
<u>Star B</u>				
1	Recoil	76	~ 0	
2	π	347	+79	610±50
3	Recoil	301	+13	
4	π	186	-59	440±190

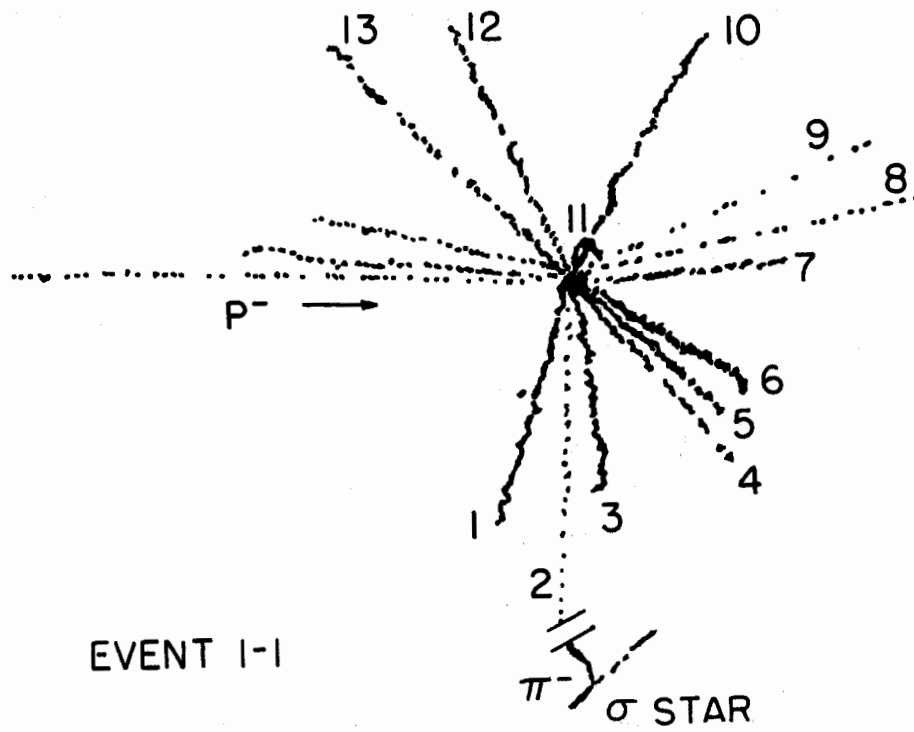


MU-12131

Fig. A.4

Table A. V. Characteristics of the tracks in Event 1-1:
annihilation in flight ($T_{p^-} = 185$ Mev), giving two charged pions

Track	Type	Projected angle (degrees)	Dip angle (degrees)	E (Mev)
1	p	73	- 49	17.3
2	π^-	89	+ 16	215
3	p	96	+ 26	10.7
4	p	135	+ 8	67.0
5	p	137	+ 49	29.5
6	p	150	- 37	22.5
7	p	194	- 33	68.0
8	p	205	+ 39	104.5
9	π	242	+ 25	247
10	p	262	+ 25	11.8
11	p	234	- 64	16.7
12	p	297	- 8	12.8
13	p	218	- 1	28.3
14	p	249	+ 28	15.8
15	p	0.4	+ 49	13.3

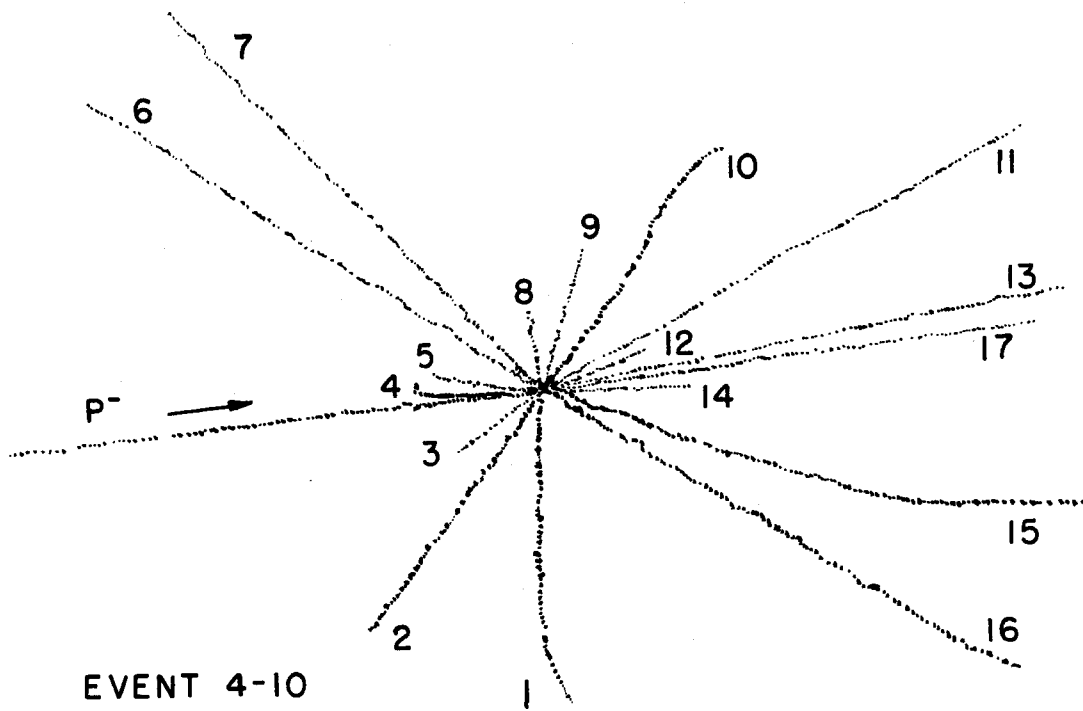


MU-12132

Fig. A.5

Table A. VI. Characteristics of tracks in Event 4-10:
annihilation in flight ($T_{p^-} = 1200 \text{ Mev}$), giving one charged pion

Track	Type	Projected angle (degrees)	Dip angld (degrees)	E (Mev)
1	p	83	- 58	16
2	p	49	+ 10	28
3	p	39	+ 39	51
4	p	3	+ 28	13.5
5	p	338	+ 47	12.5
6	p	324	+ 0.5	100
7	p	309	(- 0)	55
8	p	277	+ 58	45
9	p	257	+ 17	17
10	p	232	- 16	13.5
11	p	206	- 75	283±30
12	α	202	+ 51	43
13	p	188	- 7	51
14	p	179	+ 26	39
15	p	155	- 56	52
16	p	141	+ 8	16
17	π	183	- 14	380±50

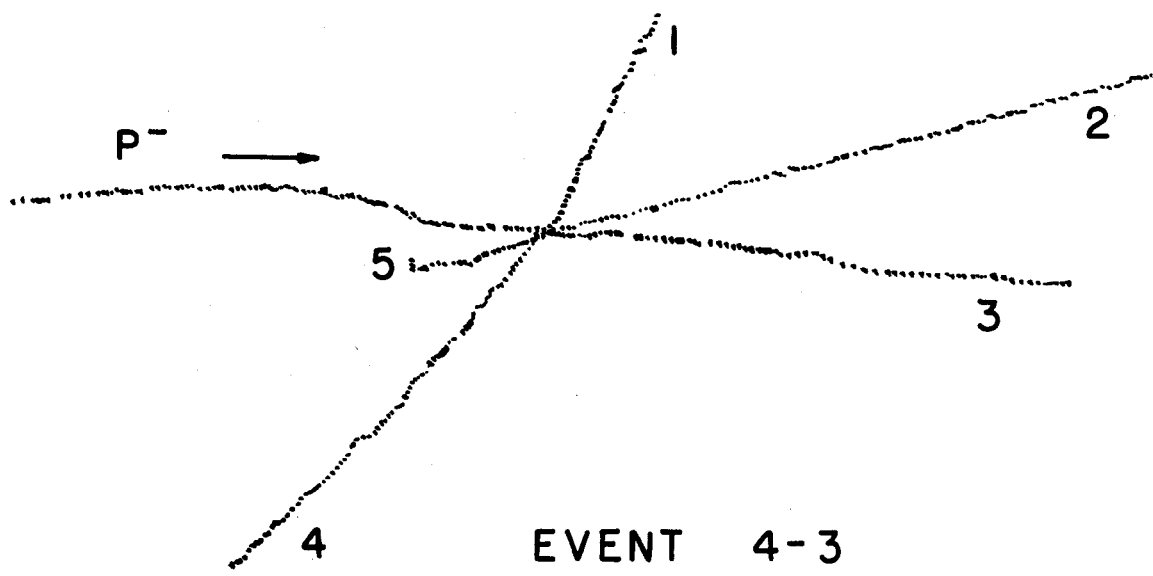


MU-12133

Fig. A.6

Table A. VII. Characteristics of tracks from Event 4-3:
annihilation at rest, giving no charged pions

Track	Type	Projected angle (degrees)	Dip angle (degrees)	E (Mev)
1	α	215	+ 38	16
2	p	353	- 1.5	10
3	p	6	- 58	10.5
4	p	135	- 56	11
5	p	164	+ 38	25

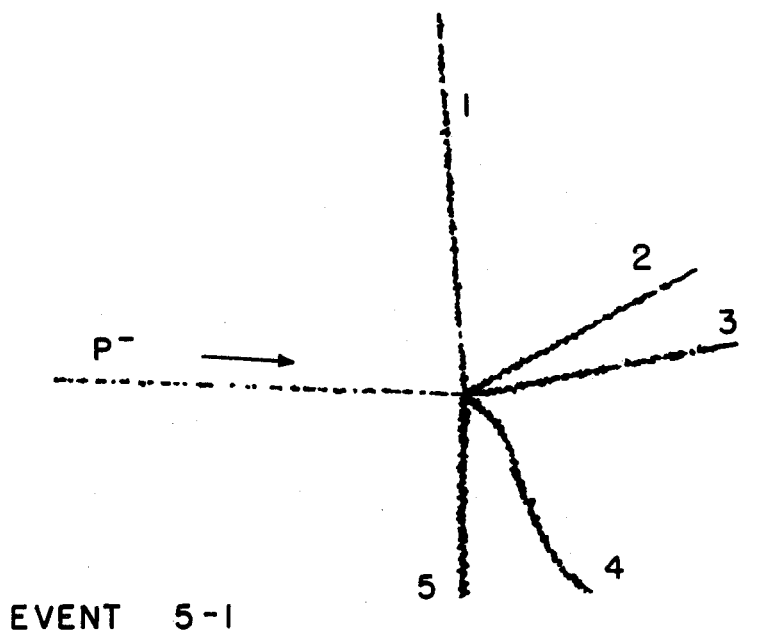


MU-12134

Fig. A.7

Table A. VIII. Characteristics of tracks from Event 5-1:
annihilation in flight ($T_p = 150$ Mev), giving no charged pions;
possible charge exchange

Track	Type	Projected angle (degrees)	Dip angle (degrees)	E (Mev)
1	p	65	- 22	35.3
2	p	143	+ 65	12.2
3	p	156	+ 65	18.6
4	p	209	- 81	15.1
5	p	269	- 40	10



MU-12218

Fig. A.8

Appendix II. Evidence for K-Meson Production

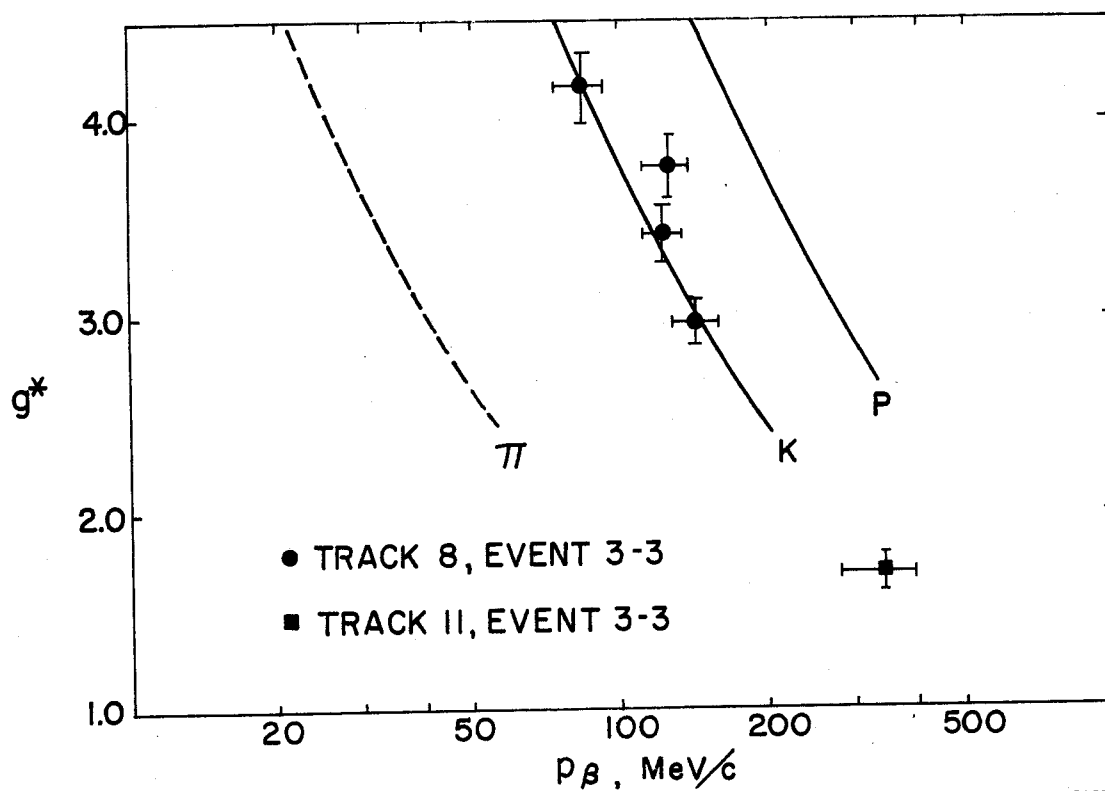
A. Gösta Ekspong and Gerson Goldhaber

1. Event 3-3: Evidence for the Production of a $K\bar{K}$ Meson Pair in the Annihilation Process

Event 3-3 was caused by an antiproton in flight, $T_{p^-} = 183$ Mev. The star consists of 7 black tracks, probably due to protons; one recoil track; two tracks of minimum ionization, probably due to π mesons; and two grey tracks, one of which is definitely due to a K meson and the other probably also due to a K meson. This star is the only one in which we have evidence for a charged $K\bar{K}$ meson pair. The first K meson, track No. 8, disappears in flight in the middle of one emulsion after a traversed path of 24.7 mm. We have not been able to find any connecting track, as we should had the K meson decayed in flight. It is most probable that the K meson underwent a charge-exchange scattering or an absorption without leaving any visible prongs. The other track, tentatively assigned to a K meson, track No. 11, left the stack after a traversed path of 40 mm.

The most serious systematic error in mass measurements by the multiple scattering-ionization method is caused by emulsion distortion. Such distortion lowers the apparent mass of particles. For track No. 8 in star 3-3 rather favorable conditions prevailed. The dip angle was between 11° and 17° in the various plates in which measurements were performed. The kinetic energy of the particle was rather low, so that small cells (25μ to 150μ) could be used for the scattering measurements. Under these two favorable circumstances distortion does not seriously affect the measurements of the multiple scattering. The final results of g/g_0 and $p\beta$ determinations are shown in Fig. A.9. The following corrections have been made: dip corrections, noise elimination between cell t and cells $2t$ and $3t$, variation of sensitivity between plates and with depth below the surface in each plate. The appropriate scattering constant K_0 was taken from Pickup and Voyvodic.²² The gap coefficient $g^* = g/g_0$ has been normalized to minimum ionization by use of the 700-Mev/c π mesons readily available in the stack. The lines marked K and P in Fig. A.9 were determined by accurate calibrations on K mesons (from a K-meson stack) and protons (from both the K-meson and the antiproton stacks). Multiple-scattering measurements were performed over the entire length of the track. The mass

²²L. Voyvodic and E. Pickup, Phys. Rev. 85, 91 (1952).



MU-12135

Fig. A.9

of the particle, according to these measurements, is $M = 1016 \pm 120 m_e$, where an 8% uncertainty in the scattering constant has been included in the standard errors. A mass determination independent of the multiple-scattering measurements can be obtained in this case by studying the variation of g/go with range (Fig. A.10). It is evident from Fig. A.10 that the measurements are consistent with the K mass and not the proton or π mass. Using the first and last points, we obtain a mass of $800^{+300}_{-200} m_e$. Our conclusion from the evidence presented here is that we have observed the emission of a K meson from an antiproton annihilation reaction.

The other grey track in the same star, track No. 11, for which the identification is less certain, was emitted with a large dip angle (74°). The surface-angle method (see Appendix IV) was applied to determine $p\beta$, and the gap-coefficient method was used for g/go . The results are shown in Fig. A.10 and also in Fig. A.11 where g/go has been converted into B/Bo (blob density). The curves in Fig. A.11 marked P and π have been obtained by calibration measurements on flat tracks of protons and π mesons in the same stack. If we assume that no appreciable undetected systematic errors enter these measurements, we see that the results indicate a K-particle mass.

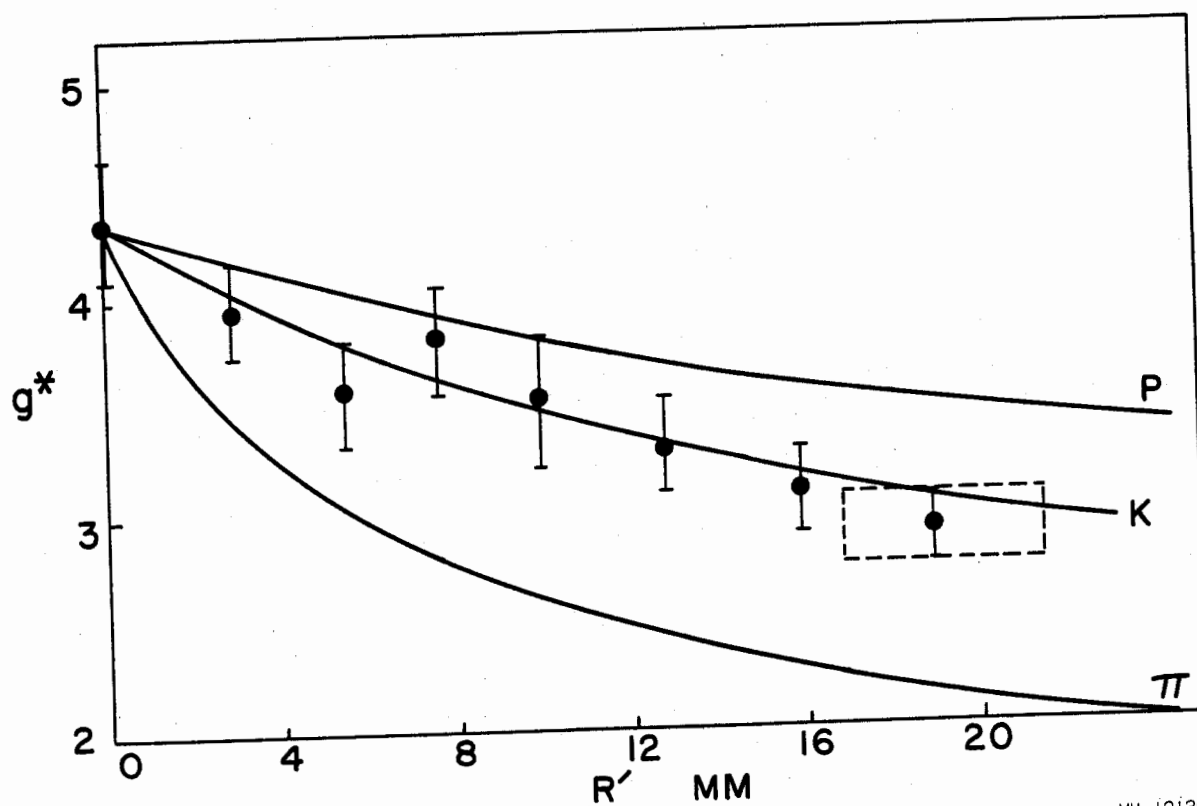
Table A. IX gives the results of the measurements on star 3-3, and Fig. A.12 gives a projection drawing of it.

If the recoil track (4) is excluded, the momentum unbalance in this star is 920 Mev/c, which is directed approximately opposite to track No. 4. Assuming the momentum of the recoil particle (track No. 4) to be about 200 Mev/c, we find that the missing momentum is about 700 Mev/c and the missing energy about 220 Mev. These quantities can be balanced by the emission of one or more neutrons. Thus momentum and energy can be conserved in this analysis, which takes track No. 11 to be due to a K meson.

2. Event 3-7: Evidence for the Emission of One Charged K Meson from an Annihilation Star

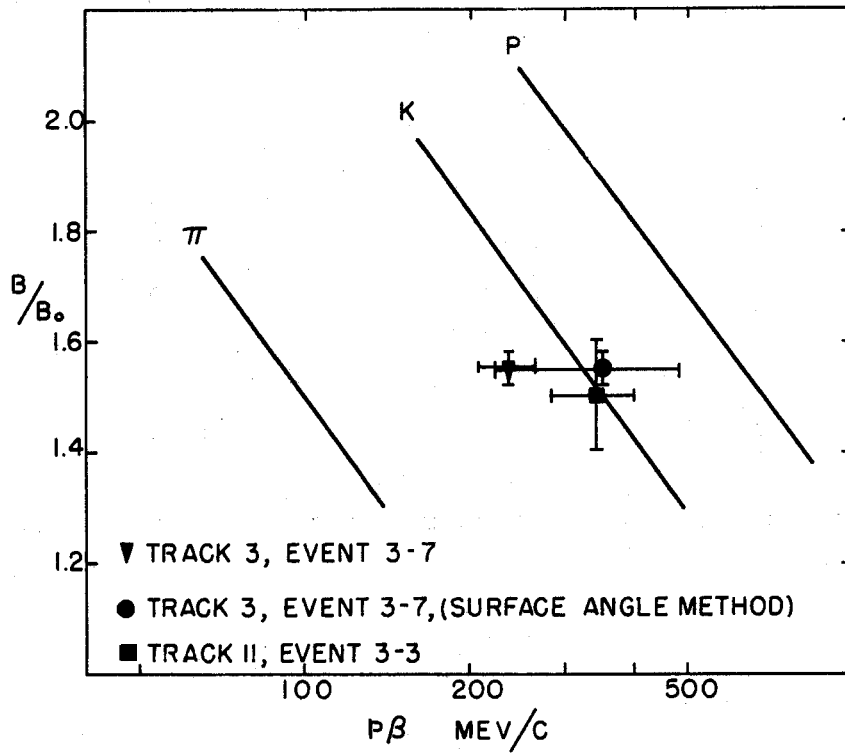
In this event track No. 3 is probably a K meson that left the stack after traversing 17 plates. Accurate blob counts on track No. 3 were made in seven plates, giving the initial $B/Bo = 1.51 \pm 0.04$, and before leaving the stack the final $B/Bo = 1.59 \pm 0.04$. As an average over the whole track we take $B/Bo = 1.55 \pm 0.03$. The average dip angle was 18° . Measurement of the multiple scattering was made over the entire track with cells of 100, 200, and 300μ . Unfortunately, distortion entered into the measurements, so that

the second differences yielded too low a $p\beta$ value ($p\beta = 160 \pm 18 \text{ Mev}/c$) as compared with that from third differences ($p\beta = 238 \pm 30 \text{ Mev}/c$). As a check, a $p\beta$ value from fourth differences was also computed, viz., $p\beta = 196 \pm 35 \text{ Mev}/c$. Utilizing the surface angle method (Appendix IV), we obtained a value of $p\beta = 350 \pm 130 \text{ Mev}/c$. The results are displayed in Fig. A.11. The mass from the third difference measurements is $M = 720 \pm 135 m_e$, and from surface angles $M = 1060^{+540}_{-440} m_e$ and is thus consistent with the K mass. The error stated is the standard error. A full description of Event 3-7 is given in Table A. X, and a projection drawing in Fig. A.13.



MU-12136

Fig. A.10

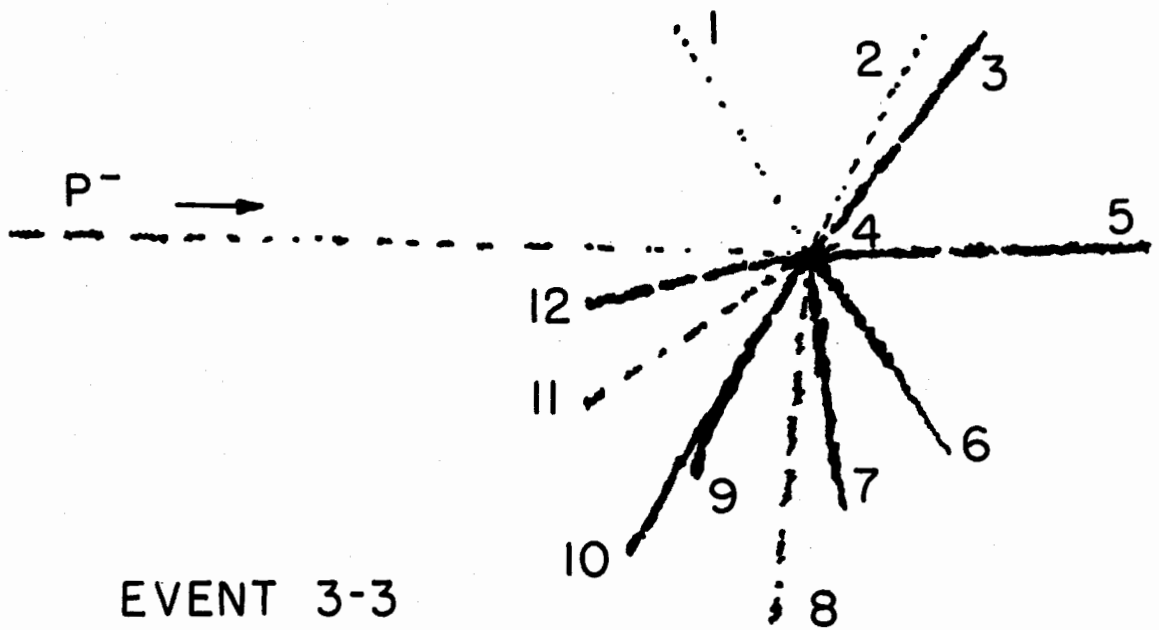


MU-12137

Fig. A.11 .

Table A. IX. Characteristics of tracks from Event 3-3:
annihilation in flight ($T_{p^-} = 183$ Mev), giving two charged K mesons and
two charged pions $T_p = 183$ Mev

Track	Type	Projected angle (degrees)	Dip angle (degrees)	E (Mev)
1	π	238	- 58	230±50
2	π	295	+ 65	240±50
3	p	306	+ 58	17
4	recoil	345	~ 0	--
5	p	357	- 52	26
6	p	53	- 39	13
7	p	81	- 36	23
8	K	93	- 15	570
9	p	119	+ 45	15
10	p	120	+ 18	12
11	K	144	+ 74	690
12	p	165	- 40	21

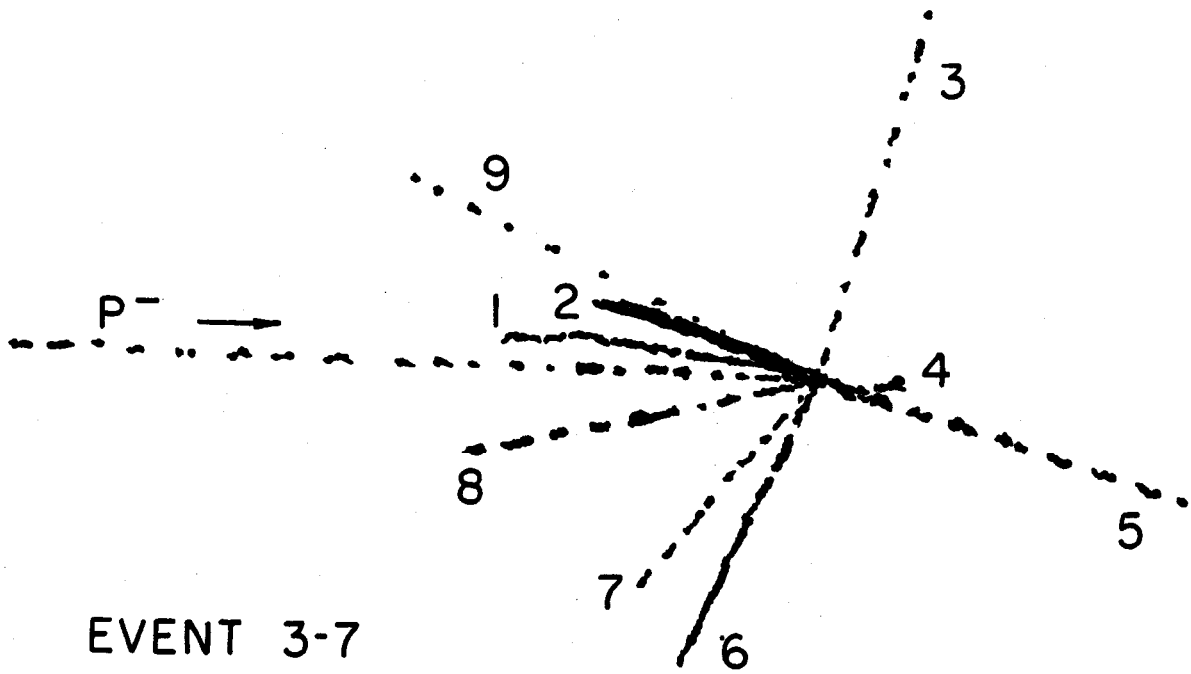


MU-12138

Fig. A.12

Table A. X. Characteristics of the tracks from Event 3-7:
annihilation in flight ($T_{p^-} = 152$ Mev), giving one charged K meson
and 2 charged pions

Track	Type	Projected angle (degrees)	Dip angle (degrees)	E (Mev)
1	p	172	- 32	17.5
2	α	168	+ 36	16.5
3	K	76	+ 19	680
4	p	346	0	9
5	p	346	- 3	45
6	p	247	0	11
7	π	232	+ 67	192 \pm 13
8	p	194	+ 20	48
9	π	157	- 17	275 \pm 22



EVENT 3-7

MU-12139

Fig. A.13

Appendix III. Annihilation Accompanied by K-Particle Production
and with Accountable Energy and Momentum

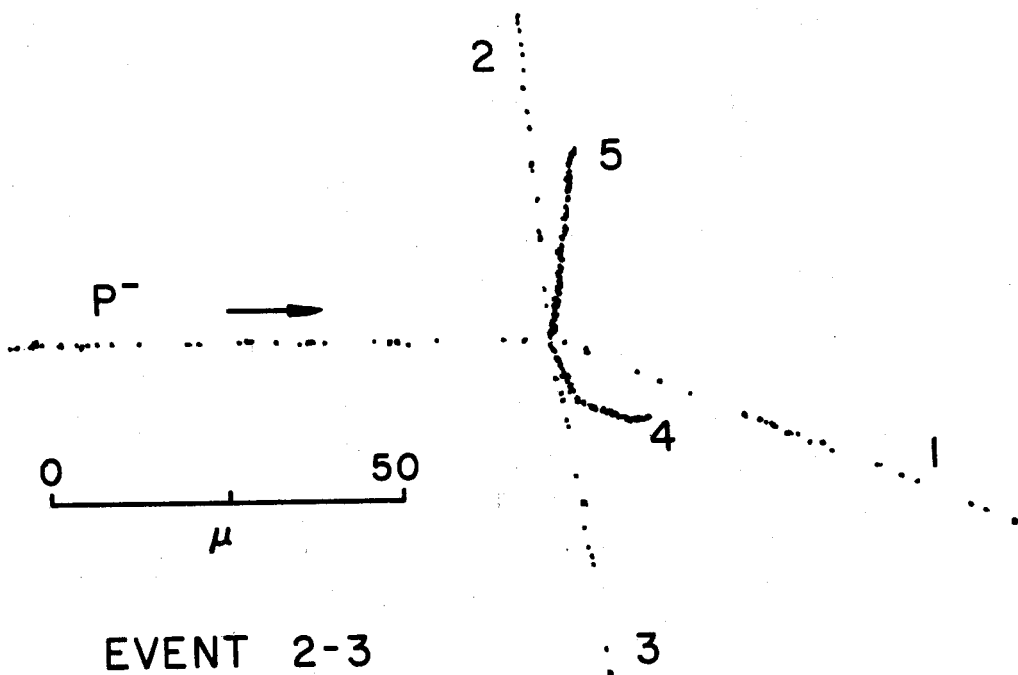
Harry H. Heckman

Event 2-3

In this nuclear interaction of a 90 ± 10 Mev antiproton, one of the five charged prongs emitted from the annihilation is probably a K meson. The event is of further interest in that it is the only annihilation star observed in this study to contain an energetic highly charged fragment. The conservation of energy and momentum can be satisfied with the emission of a single neutral particle of near nucleonic mass if one assumes that the annihilation takes place in one of the light nuclei in the emulsion and that the total energy release in the annihilation process is $2M_p c^2$.

The event is reproduced in Fig. A. 14. Of the three prongs requiring mass determination by ionization and multiple scattering, only track No. 1 had a dip angle small enough (6.2°) to allow a measure of $p\beta$ by conventional methods. Tracks 2 and 3 were nearly colinear, and had dip angles of 45.8° and -41.3° respectively. For these particles, the method of surface angles was employed to measure the multiple scattering (see Appendix IV). The ionizations of prongs Nos. 1 to 3 relative to minimum was obtained by comparing them with the 700-Mev/c incident beam pions. As a check on the grain counts of the steeply diving tracks, the ionization plateau was measured (by use of "background" $\mu^+ - e^+$ decays) as a function of dip angle. Prong 4 is a singly charged particle (p or d), and prong No. 5 is a nuclear fragment with an estimated Z of about 5. Since no particle was observed to be emitted at the end of its range, we concluded that the fragment was a nucleus stable against β decay. Table A. XI gives the results of the analysis of the event. Columns (b) and (c) are the projected and dip angles measured relative to the direction of the incident antiproton, and Column (d) gives the total path length observed for each particle. Only Prongs 4 and 5 come to rest in the emulsion stack. The identifications of particles Nos. 1 and 3 were deduced from Fig. A. 15. The expected loci of pions, K mesons, protons, and charged hyperons were calculated by use of the tables of Barkas and Young.²³ Included in the figure are several nonrelated particles used for calibration purposes. The mass of

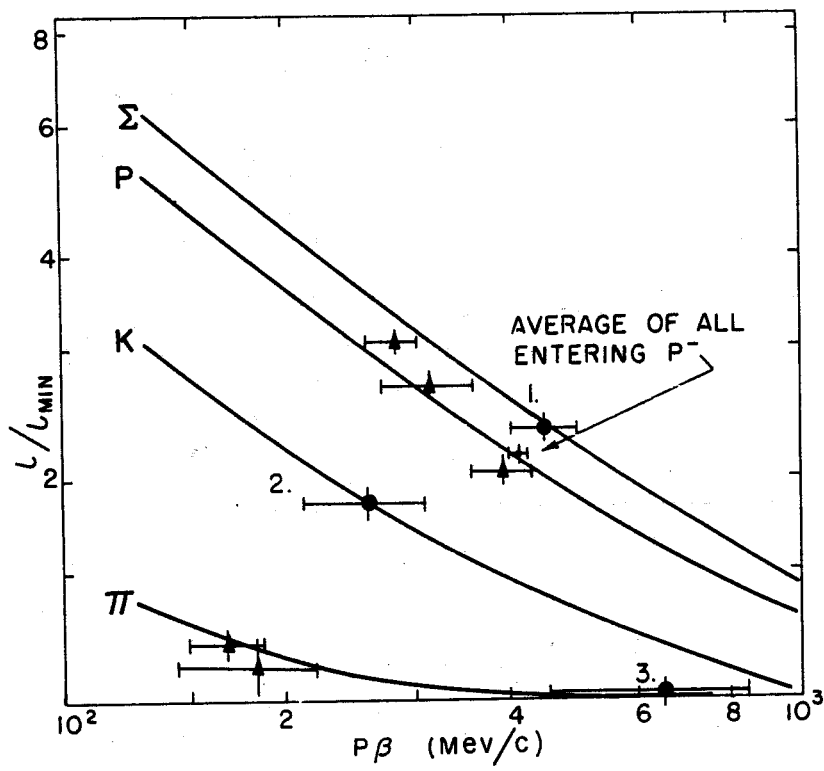
²³W. H. Barkas and D. M. Young, Emulsion Tables. I. Heavy-Particle Functions, UCRL-2579 (Rev), Sept. 1954.



EVENT 2-3

MU-12140

Fig. A.14



MU-12141

Fig. A.15

Table A. XI. Tabulation of data from the analysis of Event 2-3

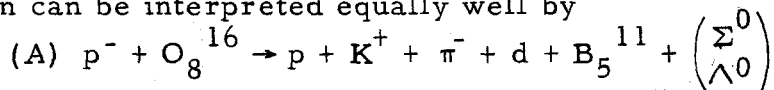
(a)	(b)	(c)	(d)	(e)	(f)	(g)	(h)	(i)	(j)
Prong	α (de- grees)	β (de- grees)	Range (ob- served) (cm)	ι/ι_{\min}^a	$p\beta$ (Mev/c)	Kinetic energy (Mev)	PC (Mev)	Mass (Mev)	Type
1	22	6.2	4.2	2.33 ± 0.07	448 ± 40	$245 \pm 24(\Sigma)$ $250 \pm 25(p)$	$804 \pm 43(\Sigma)$ $729 \pm 41(p)$	1172 ± 104	$\Sigma(p)$
2	255.5	44.3	1.89	1.88 ± 0.06	259 ± 44	146 ± 37	407 ± 53	490 ± 83	K
3	80.5	-41.3	2.39	1.00 ± 0.02	650 ± 200	650 ± 192	664 ± 197	140 ± 43	π
4	65.5	-0.3	19.5 ± 0.5	-	-	7.1 ± 1.2	163.5 ± 14.0	-	d
5	275.5	0.4	26.0 ± 0.5	-	-	23.6 ± 0.5	695 ± 8	-	B_5^{11}
p^-	0.0	0.0				90 ± 10^b	422 ± 24		

^aThe restricted grain density relative to minimum, ι/ι_0 , defined in Reference 1.

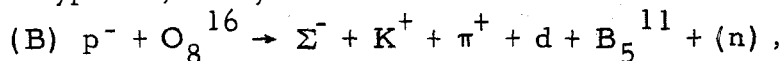
^bThe p^- had $\approx 2.5 \pm 0.5$ cm residual range at the point of interaction, corresponding to a kinetic energy of 90 ± 10 Mev.

prong No. 1 appears to be slightly larger than a proton, and it may be tentatively identified as a Σ particle. The fact that no decay was observed in a proper time of 3×10^{-10} second ($\tau_{\Sigma^-} = 1.4_{-0.5}^{+1.6} \times 10^{-10}$ sec)²⁴ slightly weakens this argument. The error of the measurement, however, does not allow the particle to be statistically resolved from the proton locus. Track 2 gives strong evidence of a K particle and Track 3 is identified as that of a pion.

The features of this event are those characteristic of an interaction with a light nucleus (C, N, or O). The evidences for this are the low kinetic energies of the stopping particles Nos. 4 and 5. In each case, the energies are considerably lower than the Coulomb-barrier heights for the heavier elements contained in emulsion. On the basis of these arguments, the annihilation can be interpreted equally well by



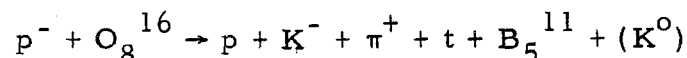
where prong No. 1 is assumed to be a proton and the unobserved neutral particle a hyperon; or by



where prong No. 1 is assumed to be a Σ^- , and the neutron is added to conserve nucleons, energy, and momentum.

In Reaction (A), the total energy unbalance ΔE of the visible charged particles is 1265 ± 197 Mev. The unbalance in momentum is 388 ± 76 Mev/c. The rest mass of a neutral particle that satisfies these values of energy and momentum is $M = 1024 \pm 182$ Mev. This evaluation of the mass from the measured quantities is in close agreement with the assumed neutral hyperon, Σ^0 or Λ^0 , emitted in the reaction (the masses of the Σ^0 and Λ^0 are 1196 ± 3 and 1116 ± 1 Mev, respectively). The Σ^0 mass is taken to be the same as the mass of the Σ^- .

If one takes the mass measurement of particle No. 1 at face value (so that we interpret it as a Σ particle), Reaction (B) can describe the annihilation. The total energy and momentum required to conserve these quantities are 1009 ± 197 Mev and 458 ± 57 Mev/c. The mass of the neutral particle is calculated to be 899 ± 192 Mev, and, within the error, is the mass of the assumed neutron (939.5 Mev). A reaction of the type



²⁴J. Steinberger, Proceedings of Sixth Annual Rochester Conference, 1956, (to be published).

does not lead to a satisfactory interpretation. The total energy unbalance is 329 ± 200 Mev (mass of $K^0 \approx 493$ Mev), and $\Delta p = 399 \pm 7$ Mev/c, from which the mass of the neutral particle is deduced to be \approx zero.

The analysis of the event does not enable one to distinguish between the modes through which the annihilation could have taken place, namely, the creation of a $\pi - \pi$ pair or a $K - \bar{K}$ pair. In either case, however, one member of the pair necessarily interacts with the remaining nucleus to produce the observed products. For instance, the positive pion could interact to produce the K^+ particle and neutral hyperon in Reaction (A), or alternatively, the interaction of the K^- with a proton could give rise to the Σ^- and π^+ in Reaction (B). The mechanism through which the recoiling B_5^{11} fragment attained its exceptionally high momentum of 695 ± 8 Mev/c might be explained by such a secondary interaction of a primary annihilation product.

Appendix IV. Measurements of Multiple Scattering on Steep Tracks

Much information would be lost in the analysis of antiproton stars if no measurements were made on the frequently occurring steep tracks. As is well known, the usual methods of evaluating the multiple scattering become quite unreliable for steep tracks because of the influence of the emulsion distortion and also because of the limited track length in each plate.

We have tried two modifications of current techniques, i. e., the sagitta and tangent methods. We will call these modifications the grid-coordinate and the surface-angle methods, respectively. Both methods are applicable to steep tracks in well-aligned emulsion stacks.

A. The Grid-Coordinate Method

Before mounting, a millimeter grid is contact-printed on the glass-to-emulsion interface of each emulsion sheet in such a way that corresponding grid coordinates on all the plates are accurately positioned atop one another.²⁵ The x and y coordinates of the glass exit or entrance point of the track are measured with respect to those grids.

The second differences of the x readings and y readings give two independent measures of the scattering. The reproducibility of the setting on a grid line is about 2 microns. The intrinsic errors in the technique arise from misalignment errors in the stack and from the variation of the original thickness of the pellicles. The total error due to these sources is about 9 microns in y and 6 microns in x. The basic cell t is the track length in each plate. By computing the scattering result in cell lengths of nt (n = 1, 2, 3, ...), one gets estimates of both the noise level and the true scattering. The formulas used to evaluate the mean scattering angle per 100-micron cell, $\bar{\alpha}_{100}$, are:

$$\bar{\alpha}_{100} = \frac{180}{\pi} \frac{1}{(t/100)^{1/2}} \frac{\langle |\Delta^2 y| \rangle}{t} \frac{\sin \beta}{\sqrt{1 - \cos^2 \theta \cos^2 \beta}}$$

and

$$\bar{\alpha}_{100} = \frac{180}{\pi} \frac{1}{(t/100)^{1/2}} \frac{\langle |\Delta^2 x| \rangle}{t} \frac{\sin \beta}{\sqrt{1 - \sin^2 \theta \cos^2 \beta}},$$

²⁵Goldhaber, Goldsack, and Lannutti, Method for Alignment of Stripped Nuclear Emulsions, UCRL-2928, Mar. 1955.

where t is the cell length in microns, β is the true dip angle, and θ the azimuthal angle with respect to the grid lines.

B. The Surface-Angle Method

The practicability of this technique depends upon the assumption that the direction of a track at the surface is retained in the processed emulsion. The projected entrance angles are measured with respect to well-aligned grid lines, tabs,²⁶ or some other reference lines. As the track scatters, the variation of the projected surface angles is a measure of the multiple scattering. If $\langle \Delta\theta \rangle$ is the mean deflection in the projected angle per pellicle, then the mean scattering angle per 100-micron cell, $\bar{\alpha}_{100}$ is given by

$$\bar{\alpha}_{100} = \langle \Delta\theta \rangle \frac{\cos\beta \sin^{1/2}\beta}{(T/100)^{1/2}},$$

where β is the dip angle and T is the original emulsion thickness in microns. The evaluation of the "noise level" was performed by studying the dependence of $\langle \Delta\theta \rangle$ on cell lengths (track length in each pellicle) in multiples of 1, 2, 3, The estimates of the noise varied between 0.25° and 0.5° in various stacks for individual $\Delta\theta$ measurements.

Although the measurements are rather difficult and limited in statistics, we feel that the methods do give satisfactory results. The reliability of the new techniques has yet to be fully explored, but as a check, we have measured the $p\beta$ of the secondaries from K mesons and slow pions having dip angles from 8° to 53° . The $p\beta$ of the secondaries from $K_{\pi 2}$ and $K_{\mu 2}$ are 165 and 214 Mev/c, respectively, and the $p\beta$ of the slow pions are known from their ranges. The results are given in Table A. XII.

A further check is obtained by comparing the π -meson energy distribution in the antiproton stars (Section IV B) for steep tracks with that for flat tracks. The two spectra show a rather good over-all agreement.

²⁶Birge, Kerth, Richman, Stork, and Whetstone, Techniques for Handling and Processing Emulsion Stacks, UCRL-2690, Sept. 1954.

Table A. XII. $p\beta$ of dipping tracks, measured by the surface-angle method

Particle	Dip angle (degrees)	$p\beta$, measured (Mev/c)	$p\beta$, known (Mev/c)
$K_{\mu 2}$ secondary	8	198 ± 35	214
$K_{\pi 2}$ secondary	53.3	166 ± 22	165
$K_{\mu 2}$ secondary	33	274 ± 55	214
\bar{p} ion	45.7	68 ± 10	76.2

Appendix V. The Lepore-Neuman Statistical Model

We start with the following expression for the probability of annihilation into N pions according to the Lepore-Neuman model.¹⁸

$$P_N = \text{const. } S_N T_N (2\pi\hbar)^{-3(N-1)} \int \prod_{i=1}^N d^3 p_i d^3 x_i \delta(W - \sum_i \epsilon_i) \delta(\sum_i \vec{p}_i) \times \\ \delta\left(\frac{\sum_i \vec{x}_i \epsilon_i}{W}\right) \exp\left[-\frac{(\tau_{\pi} x_i^2 \epsilon_i^2)}{\hbar^2 c^2}\right].$$

After the spatial integration is carried out, we obtain

$$P_N = \text{const. } S_N T_N (4\pi\tau_{\pi})^{-3(N-1)1/2} (W^3/N^{3/2}) \int \prod_{i=1}^N d^3 p_i \epsilon_i^{-3} \delta(W - \sum_i \epsilon_i) \delta(\sum_i \vec{p}_i).$$

We define an energy $\bar{\epsilon}$ by means of the expression

$$(\bar{\epsilon})^{-3N} = \frac{\int \prod_{i=1}^N d^3 p_i \epsilon_i^{-3} \delta(W - \sum_i \epsilon_i) \delta(\sum_i \vec{p}_i)}{\int \prod_{i=1}^N d^3 p_i \delta(W - \sum_i \epsilon_i) \delta(\sum_i \vec{p}_i)}.$$

For large multiplicities $\bar{\epsilon}$ approaches the pion rest mass energy. We wish to compare $\bar{\epsilon}$ with the average pion energy, W/N_{π} , at low multiplicities. Holland²¹ has evaluated the integral in the numerator of the above expression for multiplicities $N_{\pi} = 2, 3, 4$. The evaluation of the denominator has been described in Section IV G. 1. The results are shown in Table A. XIII, where $\bar{\epsilon}$ and W/N_{π} are given in pion rest energy units.

The near equality of $\bar{\epsilon}$ and the average pion energy, W/N_{π} , may at first seem surprising since the term $(\epsilon_i)^{-3}$ favors low energies. However, because of the term that provides for the conservation of energy, high energies must be equally favored. Thus the above equality is reasonable although perhaps accidental. It should be noted that the procedure described above is applicable only in cases where all particles in the final state have the same mass, as in the annihilation process involving pions only.

The expression for P_N in Section IV G. 3 has been obtained by means of the substitution $\bar{\epsilon} = W/N_{\pi}$.

Table A. XIII. Comparison between $\bar{\epsilon}$ as defined above and calculated from the results of Holland^a and the average pion energy $\frac{W}{N_\pi}$. All energies are expressed in units of $M_\pi c^2$.

N_π	$\bar{\epsilon}$	W/N_π
2	6.8	6.8
3	4.5	4.5
4	3.5	3.4
13.4	1.0	1.0

^aSee Ref. 21.

FIGURE CAPTIONS

- Fig. 1. Antiproton ranges (experimental points) as a function of the point of entry in the stack. Calculated range-momentum curves (solid lines) for particles of $0.95 M_p$, $1 M_p$, and $1.05 M_p$, respectively.
- Fig. 2. Percent opacity versus residual range for protons, deuterons, and antiprotons. Deuteron ranges have been divided by 2.
- Fig. 3. A. Observed antiproton path length versus kinetic energy. B. The number of observed annihilations in flight; number of scatters in each energy interval.
- Fig. 4. Elastic Scattering. Distribution of space angles of scattering observed in (A) 158.3 cm of antiproton track in energy interval 50 to 200 Mev, (B) 97 cm of positive proton track in energy interval 50 to 100 Mev.
- Fig. 5. Distribution in \bar{d} from constant-sagitta multiple-scattering measurements. (A) antiprotons from 0 to 150μ , (B) positive protons from 0 to 150μ , (C) positive protons from 100 to 250μ .
- Fig. 6. Visible energy release in antiproton annihilation stars, expressed as a fraction of the available energy. The star reference number is given for each entry.
- Fig. 7. Charged-pion energy spectrum from annihilation stars. (Tracks with dip angle less than 20° are represented in shaded portion.)
- Fig. 8. A. Energy spectrum of heavy particles from annihilation stars. All unidentified tracks were considered to be protons. (Spectra from stars at rest are represented in shaded portion.) B. Proton energy spectrum below 35 Mev empirically corrected by eliminating contribution of α particles. Dotted curve has been calculated from evaporation theory for $U_{EV} = 170$ Mev.
- Fig. 9. The distribution of the visible energy in heavy prongs per star. The arrows indicate the expected visible energy release in heavy prongs due to the absorption of 1, 2, or 3 pions. (For average pion total energy of 322 Mev.) The upper scale includes the energy given to neutrons.
- Fig. 10. Experimental distribution of pions from stars in flight vs space angle θ (lab). Theoretical curve computed for isotropic distribution in the c.m. system, averaged over antiproton energy, Fermi momentum of target nucleon, and energy of created pions.
- Fig. 11. Number of pion pairs as a function of the angle between pairs. Theoretical curve shows distribution expected if the pions are emitted independently.

- Fig. 12. Distribution of the observed charged-pion multiplicity (from annihilation stars). Stars at rest are represented by shaded portion.
- Fig. 13. Pion energy spectrum. Histogram shows experimentally found charged-pion spectrum. Solid curves are computed from the Fermi statistical model for pion multiplicities of 4, 5, 6, and 7.
- Fig. A. 1. Projection drawing of annihilation star for Event 3-13, giving five charged pions.
- Fig. A. 2. Projection drawing of annihilation star for Event 4-8, giving four charged pions.
- Fig. A. 3. Projection drawing of annihilation star for Event 1-2, giving three charged pions.
- Fig. A. 4. Projection drawing of annihilation star for Event 3-2, giving two charged pions, inelastic scattering of p^- .
- Fig. A. 5. Projection drawing of annihilation star for Event 1-1, giving two charged pions.
- Fig. A. 6. Projection drawing of annihilation star for Event 4-10, giving one charged pion.
- Fig. A. 7. Projection drawing of annihilation star for Event 4-3, giving no charged pions.
- Fig. A. 8. Projection drawing of annihilation star for Event 5-1, giving no charged pions, possible charge exchange.
- Fig. A. 9. Ionization vs multiple-scattering measurements on Tracks 8 and 11, Star 3-3. g^* is the gap coefficient as normalized to minimum ionization (700 Mev/c π mesons).
- Fig. A. 10. Ionization vs variation in range for Track 8, Star 3-3. The curves are those expected for protons, K mesons, and π mesons normalized to the value of g^* at the point of disappearance in flight of track 8. ($g^* = 4.37$). The mass determination was carried out for the first and last points. The width of the rectangle at $R' = 18$ mm indicates the uncertainty in range due to the error in g^* for the point at $R' = 0$.
- Fig. A. 11. Blob density vs $p\beta$ measurements on Track 3 in Star 3-7 and Track 11 in Star 3-3.
- Fig. A. 12. Projection drawing of annihilation star for Event 3-3, giving two K mesons, two pions.
- Fig. A. 13. Projection drawing of annihilation star for Event 3-7, giving one K meson, one pion.

Fig. A. 14. Projection drawing of annihilation star for Event 2-3, showing 1 K meson, 1 pion.

Fig. A. 15. Ionization versus multiple scattering measurements on calibration pions and protons and Tracks 1, 2, and 3 in Event 2-3.